ARTICLE

A loop extrusion–independent mechanism contributes to condensin I–mediated chromosome shaping

Kazuhisa Kinoshita[1] , Yuko Tsubota[2] , Shoji Tane[1], Yuuki Aizawa[1], Ryota Sakata[2] , Kozo Takeuchi[1], Keishi Shintomi[1] , Tomoko Nishiyama[2], and Tatsuya Hirano[1]

Condensin I is a five-subunit protein complex that is central to mitotic chromosome assembly in eukaryotic cells. Despite recent progress, its molecular mechanisms of action remain to be fully elucidated. By using *Xenopus* egg extracts as a functional assay, we find that condensin I complexes harboring mutations in its kleisin subunit CAP-H produce chromosomes with confined axes in the presence of topoisomerase IIα (topo IIα) and highly compact structures (termed "beans") with condensin-positive central cores in its absence. The bean phenotype depends on the SMC ATPase cycle and can be reversed by subsequent addition of topo IIα. The HEAT repeat subunit CAP-D2, but not CAP-G, is essential for the bean formation. Notably, loop extrusion activities of the mutant complexes cannot explain the chromosomal defects they exhibit in *Xenopus* egg extracts, implying that a loop extrusion–independent mechanism contributes to condensin I–mediated chromosome assembly and shaping. We provide evidence that condensin–condensin interactions underlie these processes.

Introduction

Mitotic chromosome assembly is a fundamental process that ensures faithful segregation of genetic information in all eukaryotic species. Chromatin within the interphase nucleus undergoes a series of dynamic structural changes upon mitotic entry and is eventually converted into a set of rod-shaped chromosomes by metaphase. Increasing lines of evidence have fully established that a class of large protein complexes, known as condensins, play a central role in the process of mitotic chromosome assembly (Hirano, 2016; Uhlmann, 2016; Paulson et al., 2021). Most eukaryotic cells have two different condensin complexes, condensin I and condensin II, each of which consists of five subunits. The two complexes share the same pair of structural maintenance of chromosomes (SMC) ATPase subunits (SMC2 and SMC4) and contain different sets of non-SMC subunits. SMC2 and SMC4 form a V-shaped dimer, and their head domains are bridged by a kleisin subunit (chromosome-associated polypeptide [CAP]-H in condensin I and CAP-H2 in condensin II). The kleisin subunit is then bound by a pair of HEAT repeat subunits (CAP-D2 and -G in condensin I and CAP-D3 and -G2 in condensin II). The central role of condensins in mitotic chromosome assembly has further been substantiated by a chromosome reconstitution assay using purified components

(Shintomi et al., 2015) and a modified *Xenopus* egg cell-free extract that enables assembly of nucleosome-depleted chromosomes (Shintomi et al., 2017).

Various models have been proposed for the mechanism of action of condensins in mitotic chromosome assembly, including a diffusion capture/stochastic interaction model (Cheng et al., 2015; Gerguri et al., 2021), a supercoiling-based model (Hirano, 2014), and a model involving condensin–condensin interactions (Sakai et al., 2018; Yoshimura and Hirano, 2016). Among them, a loop extrusion model has attracted much attention during the past several years (Nasmyth, 2001; Alipour and Marko, 2012; Goloborodko et al., 2016a,b). According to this model, condensin binds to a chromatin fiber and "extrudes" a loop from its binding site. Conceptually, this model best explains how condensins make a DNA loop by exclusively forming bridges between DNA segments derived from the same chromosome (action in cis) and avoid cross-linking DNA segments derived from different chromosomes (action in trans). Elegant computer simulations (Goloborodko et al., 2016a) and high-throughput chromosome conformation capture data (Gibcus et al., 2018) are consistent with the loop extrusion model. Most important, single-molecule assays have demonstrated that yeast condensin does have the

[1]Chromosome Dynamics Laboratory, RIKEN, Wako, Saitama, Japan; [2]Division of Biological Sciences, Graduate School of Science, Nagoya University, Nagoya, Japan.

Correspondence to Tatsuya Hirano: hiranot@riken.jp; K. Takeuchi's present address is Hamamatsu Photonics K.K., Hamamatsu, Shizuoka, Japan.

ability to translocate along a DNA (Terakawa et al., 2017) and to extrude a DNA loop (Ganji et al., 2018) in an ATP hydrolysis–dependent manner. It has also been shown that human condensins I and II display loop extrusion activities in vitro (Kong et al., 2020).

Apart from this line of exciting progress, biochemical and structural studies have started to shed light on the dynamic architecture of the condensin complexes and the functional cross-talk among their individual subunits. Our previous study using *Xenopus* egg cell-free extracts as a functional assay demonstrated that the two HEAT repeat subunits of condensin I, CAP-D2 and -G, have antagonistic functions in the dynamic assembly of chromosome axes (Kinoshita et al., 2015). Structural studies using yeast condensin have identified a unique DNA binding subdomain ("safety belt") composed of Ycg1/CAP-G and Brn1/CAP-H subunits (Kschonsak et al., 2017) and revealed an asymmetric SMC ATPase cycle that involves a contact between the SMC4 head domain and Ycs4/CAP-D2 (Hassler et al., 2019). Although a "flip-flop" mechanism recently proposed based on cryo-EM data (Lee et al., 2020) could in fact provide a reasonable explanation for the antagonistic actions of the two HEAT repeat subunits (Kinoshita et al., 2015), how the dynamic and flexible conformational changes support the activities of condensin complexes is not fully understood. It also remains elusive to what extent loop extrusion contributes to folding of chromatin fibers under physiological conditions or whether the mechanism of loop extrusion alone is sufficient to assemble rod-shaped chromosomes in mitosis.

In the present study, we have reconstituted a panel of mutant complexes and tested their abilities to assemble chromosomes in *Xenopus* egg extracts. We find that mutant complexes harboring one class of mutations produce individual chromosomes with confined axes in the presence of topoisomerase IIα (topo IIα) and highly compact structures ("beans") with condensin-positive cores in its absence. The bean formation depends on the SMC ATPase and CAP-D2, but not on CAP-G. A second class of mutations causes opposing defective phenotypes in chromosome assembly. Interestingly, loop extrusion activities of the corresponding mutant complexes fail to explain the contrasting phenotypes they exhibit in *Xenopus* egg extracts, suggesting that a loop extrusion–independent mechanism contributes to condensin I–mediated chromosome assembly and shaping. Evidence that condensin–condensin interactions facilitate chromosome axis assembly is provided.

Results

CAP-H motif III mutant complexes assemble chromosomes with confined axes

The kleisin subunit CAP-H of condensin I has five motifs highly conserved among the eukaryotic orthologues (Fig. 1 A). Among the five motifs, motif I and motif V are known to interact with the SMC2 neck and SMC4 cap regions, respectively (Hassler et al., 2019), and motif II and motif IV participate in direct interactions with CAP-D2/Ysc4 and CAP-G/Ycg1, respectively (Piazza et al., 2014; Kschonsak et al., 2017; Hara et al., 2019). In the present study, we focus on motif III, in which several

aromatic residues (tyrosine [Y], phenylalanine [F], and tryptophan [W]), along with proline (P) residues, are highly conserved. Being inspired by well-characterized examples of functional interactions between HEAT repeats and peptides containing aromatic residues (Bayliss et al., 2000, 2002; Liu and Stewart, 2005; Yoshimura et al., 2014), we substituted the six aromatic residues conserved among vertebrate CAP-H with nonaromatic polar residues, glutamines (Q), and designated this set of mutations H-III6Q. We were able to successfully reconstitute and purify holo(H-III6Q), a five-subunit holocomplex of condensin I harboring H-III6Q, suggesting that these mutations do not compromise the integrity of the condensin I complex (Fig. S1 A).

We then tested the ability of holo(H-III6Q) to assemble mitotic chromosomes in *Xenopus* egg cell-free extracts (add-back assay; Kinoshita et al., 2015). In brief, metaphase egg extracts were immunodepleted of endogenous condensins (Δcond extracts) and supplemented with either holo(WT), a holocomplex with WT subunits, or holo(H-III6Q) (Fig. 1, B and D). As expected, when *Xenopus* sperm nuclei were used as a substrate, holo(WT) supported successful assembly of a cluster of single chromatids whose axes were positive for SMC4. In striking contrast, holo(H-III6Q) failed to support assembly of individualized chromosomes, leaving a banana-shaped chromatin mass in which SMC4-positive, axis-like structures were apparently entangled with each other.

A recent study from our laboratory had demonstrated that, like *Xenopus* sperm nuclei, mouse (*Mus musculus*) sperm nuclei can be converted into clusters of single chromatids in *Xenopus* egg cell-free extracts (Shintomi et al., 2017). When the above-described experiment was repeated using mouse sperm nuclei as a substrate (Fig. 1, C and D), holo(WT) supported the assembly of individualized chromosomes as expected. To our surprise, we found that holo(H-III6Q) also assembled individualized chromosomes, although their morphological features were distinct from those of chromosomes assembled with holo(WT). In the chromosomes assembled with the mutant complex, the surfaces of the chromosomes were fuzzy and could readily be distinguished from DAPI-dense central regions. Moreover, SMC4 signals were highly confined on the central axial regions (Fig. 1 E). We also prepared an additional pair of motif III mutant complexes and found that they produce structures similar, if not identical, to those produced by holo(H-III6Q) (Fig. S1, B–H). The observations raised an interesting question of why the kleisin motif III mutant complexes exhibit apparently different defective phenotypes between the two different substrates. We suspect that chromosomal DNAs are entangled with each other more heavily in *Xenopus* sperm nuclei than in mouse sperm nuclei (see Discussion).

CAP-H motif III mutant complexes form "beans" in the absence of topo IIα

To understand how the entangled state of chromosomal DNAs affects the action of condensin I, we repeated the same set of add-back assays in the absence of topo IIα (topo II–depleted add-back assay). To this end, an extract depleted of both condensins and topo IIα was prepared (Δcond Δtopo II extracts; Fig. S1 I) and
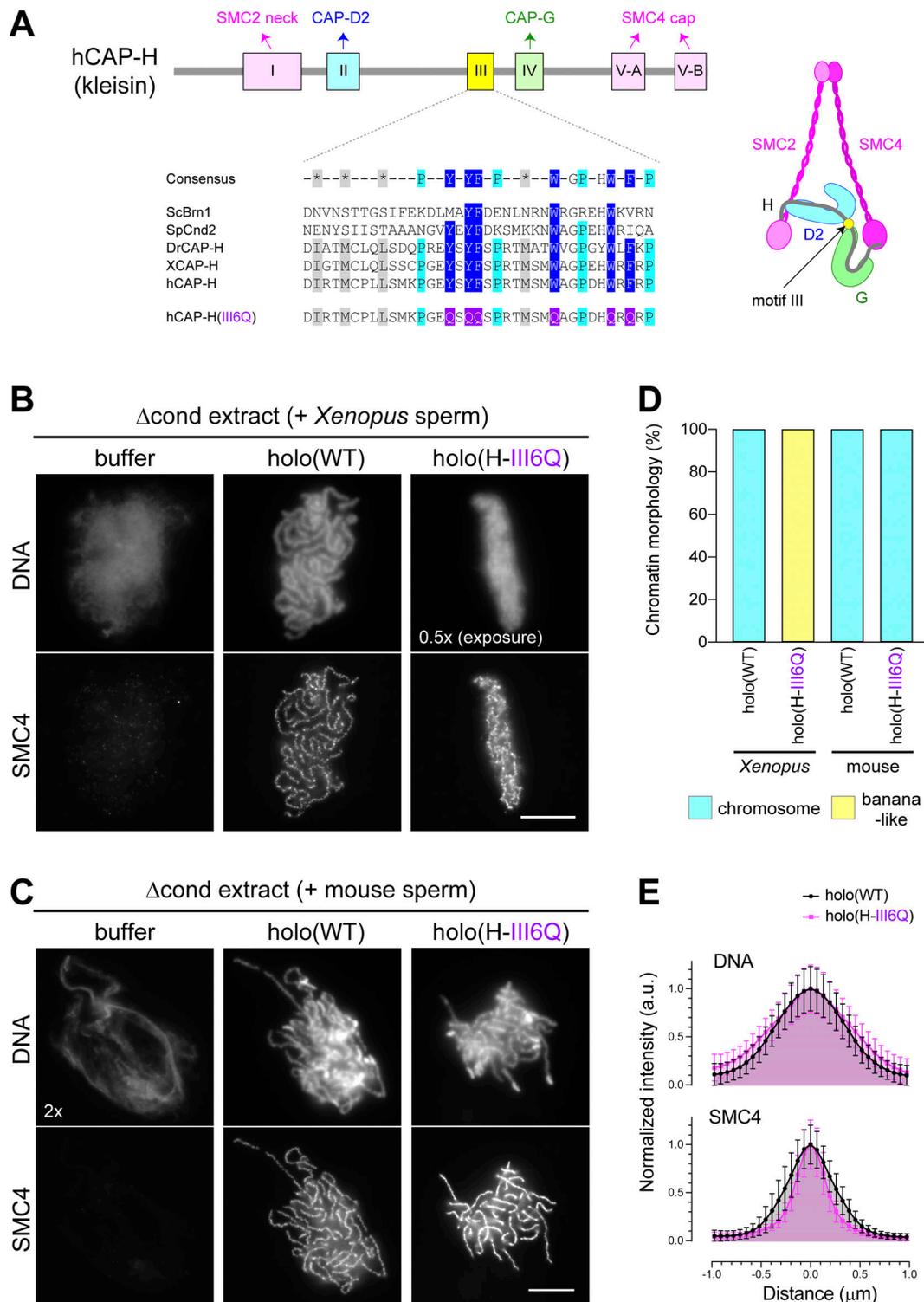
Kinoshita et al.
Chromosome shaping by condensin I

Journal of Cell Biology   2 of 17
https://doi.org/10.1083/jcb.202109016

Figure 1. **CAP-H motif III mutant complexes assemble chromosomes with confined axes. (A)** Domain organization of the CAP-H/kleisin subunit. CAP-H has five motifs that are well conserved among eukaryotic species (motifs I to V). Shown here is a sequence alignment of the CAP-H orthologues from *Saccharomyces cerevisiae* (ScBrn1), *Schizosaccharomyces pombe* (SpCnd2), *Danio rerio* (DrCAP-H), *Xenopus laevis* (XCAP-H), and human (hCAP-H). Conserved residues are labeled in dark blue (Y/F/W), light blue (P), and gray (I/M/L*). All of the six aromatic residues conserved in motif III were replaced with nonaromatic polar residues, glutamines (Q), to generate the H-III6Q mutations. A cartoon depicting the holocomplex of condensin I is shown on the right. **(B)** Add-back assay using *Xenopus* sperm nuclei as a substrate. *Xenopus* sperm nuclei were incubated with condensin-depleted (Δcond) extracts that had been supplemented with a control buffer (buffer), holo(WT), or holo(H-III6Q). After 120 min, the reaction mixtures were fixed and labeled with an antibody against SMC4. DNA was counterstained with DAPI. The DAPI image of the structure produced by holo(H-III6Q) was taken with a shorter exposure time (0.5x) than the others. The data from a single representative experiment out of four repeats are shown. Scale bar, 10 μm. **(C)** Add-back assay using mouse sperm nuclei as a substrate. Mouse sperm nuclei were incubated with the same set of extracts as described in B for 150 min and analyzed as above. A different relative exposure time (2x) was used

where indicated. The data from a single representative experiment out of three repeats are shown. Scale bar, 10 μm. **(D)** Chromosome morphology as judged by the DAPI-stained images shown in B and C. In each reaction, the morphology of the final products was highly homogeneous, displaying either "chromosome" or "banana-like" morphology (n = 38, 48, 46, and 43 from left to right). **(E)** Line profiles of chromosomes assembled from mouse sperm nuclei. The signal intensities of DNA (top) and SMC4 (bottom) of the chromosomes assembled with holo(WT) (black) or holo(H-III6Q) (magenta) were scanned along the lines drawn perpendicular to chromosome axes (n = 20). The mean and SD of 20 lines were plotted as normalized intensities (a.u.). We confirmed that there are significant differences between the holo(WT) and holo(H-III6Q) data after Gaussian curve fitting in both plots (P < 0.05 by extra sum-of-squares F test).

then supplemented with holo(WT) or holo(H-III6Q). When *Xenopus* sperm nuclei were used as a substrate, holo(WT) produced a banana-shaped chromatin mass in which SMC4 signals were uniformly distributed (Fig. 2, A and B). No sign of individualization or axis formation was observed. In contrast, holo(H-III6Q) led to formation of a small banana-shaped mass ("mini-banana") in which SMC4 signals were concentrated along the central "spine" of the mass. When mouse sperm nuclei were used as a substrate, holo(WT) produced a teardrop-shaped chromatin mass with uniform distribution of SMC4 signals (Fig. 2, C and D). Under the same condition, holo(H-III6Q) formed a compact, ball-like structure ("bean") in which SMC4 signals were highly concentrated in the central "core." We also found that, just like holo(H-III6Q), the other two motif III mutant complexes displayed the bean phenotype under the same condition (Fig. S1, J and K).

Due to the striking bean phenotype, we thereafter focused on experiments using mouse sperm nuclei in the present study. A time course of the bean formation with holo(H-III6Q) was followed (Fig. 2, E and F). At 30 min, swollen chromatin masses, each consisting of entangled chromosomal DNAs, were observed. SMC4 signals were barely detectable at this time point. At later time points (80–150 min), the size of the chromatin masses progressively got smaller. At the same time, the SMC4 signals on the chromatin masses increased and became concentrated in the central core.

In all add-back assays described above, a standard concentration of 35 nM of condensin I was used. We then tested how different concentrations of holo(H-III6Q) affect bean formation at the end time point (Fig. 2, G and H), and we found that the size of the chromatin masses decreased in a dose-dependent manner. In contrast, the size of the SMC4-positive core was relatively constant over a wide range of the holo(H-III6Q) concentrations tested, with a slight increase at high concentrations (70–105 nM). These results provide additional lines of evidence that holo(H-III6Q) indeed drives the compaction of chromosomal DNAs into a bean under the topo II–depleted condition.

The bean phenotype depends on the SMC ATPase cycle and can be reversed by subsequent addition of topo IIα
To rule out the possibility that the bean phenotype is caused by abortive aggregation of the mutant complexes, we tested the contribution of the SMC ATPase cycle to the formation of the compact structures. To this end, we combined the H-III6Q mutations with two different sets of mutations that impair the SMC ATPase cycle: Walker A mutations (mSMC2 [K38I] and mSMC4 [K117I]) block the step of ATP binding, whereas transition-state mutations (mSMC2 [E1114Q] and mSMC4 [E1218Q]) greatly slow down the rate of ATP hydrolysis (Fig. S2, A and B; Kinoshita

et al., 2015). Consistent with our previous study (Kinoshita et al., 2015), we found that SMC4 signals were not detectable on chromatin when holo(H-III6Q) harboring the SMC2-SMC4 Walker A mutations was used, whereas diffuse signals were observed when holo(H-III6Q) harboring the SMC2-SMC4 transition-state mutations was used (Fig. 3 A). In both cases, the chromatin structure remained cloudlike, and there was no sign of compaction or bean formation at all (Fig. 3 B). These results clearly demonstrated that bean formation depends on a functional SMC ATPase cycle and that the mutant condensin complex uses an active mechanism to cause the bean phenotype.

We then wished to test whether the bean morphology is a fixed product or whether it can be "reversed" by subsequent addition of topo IIα. To this end, bean structure was formed under the condition described above, and topo IIα was supplied by mixing the reaction mixture with the same volume of a condensin-depleted extract supplemented with holo(H-III6Q; Fig. S2 C). Interestingly, the bean formed in the absence of topo IIα was immediately resolved and transformed into swollen chromatin masses 10 min after the addition of topo IIα (Fig. 3 C). Further incubation converted the entangled masses of chromatin into clusters of individualized chromosomes. We also confirmed that the entangled masses of chromatin produced by holo(WT) in the absence of topo IIα could be reversed to produce clusters of individualized chromosomes (Fig. S2 D). We then followed morphological changes that occur at earlier time points in the holo(H-III6Q) reaction, and we found that the bean expanded very quickly within 5 min, during which the initially concentrated SMC4 signals gradually dispersed throughout the chromatin mass (Fig. 3, D and E). However, topo IIα signals became detectable at 1 min and accumulated over time. These results showed that the bean structure is not a fixed product and can indeed be resolved by subsequent action of topo IIα.

The bean phenotype depends on CAP-D2 but not on CAP-G
Our previous study had demonstrated that the two HEAT subunits of condensin I, CAP-D2 and CAP-G, have antagonistic functions in the dynamic assembly of chromosome axes (Kinoshita et al., 2015). In short, CAP-D2 has a positive impact on chromosome axis assembly, whereas CAP-G has a negative impact. Because the SMC4-positive core of the bean described above shares many common properties with chromosome axes, we next tested which HEAT subunit(s) might be required for bean and core formation. The H-III6Q mutations were introduced into tetramer or trimer mutant complexes that lack one or both of the HEAT subunits. The resulting mutant complexes, ΔD2(H-III6Q), ΔG(H-III6Q), and ΔD2ΔG(H-III6Q), were tested for their ability to form the bean structure in extracts depleted of condensins and topo IIα. We found that ΔG(H-III6Q) was able to
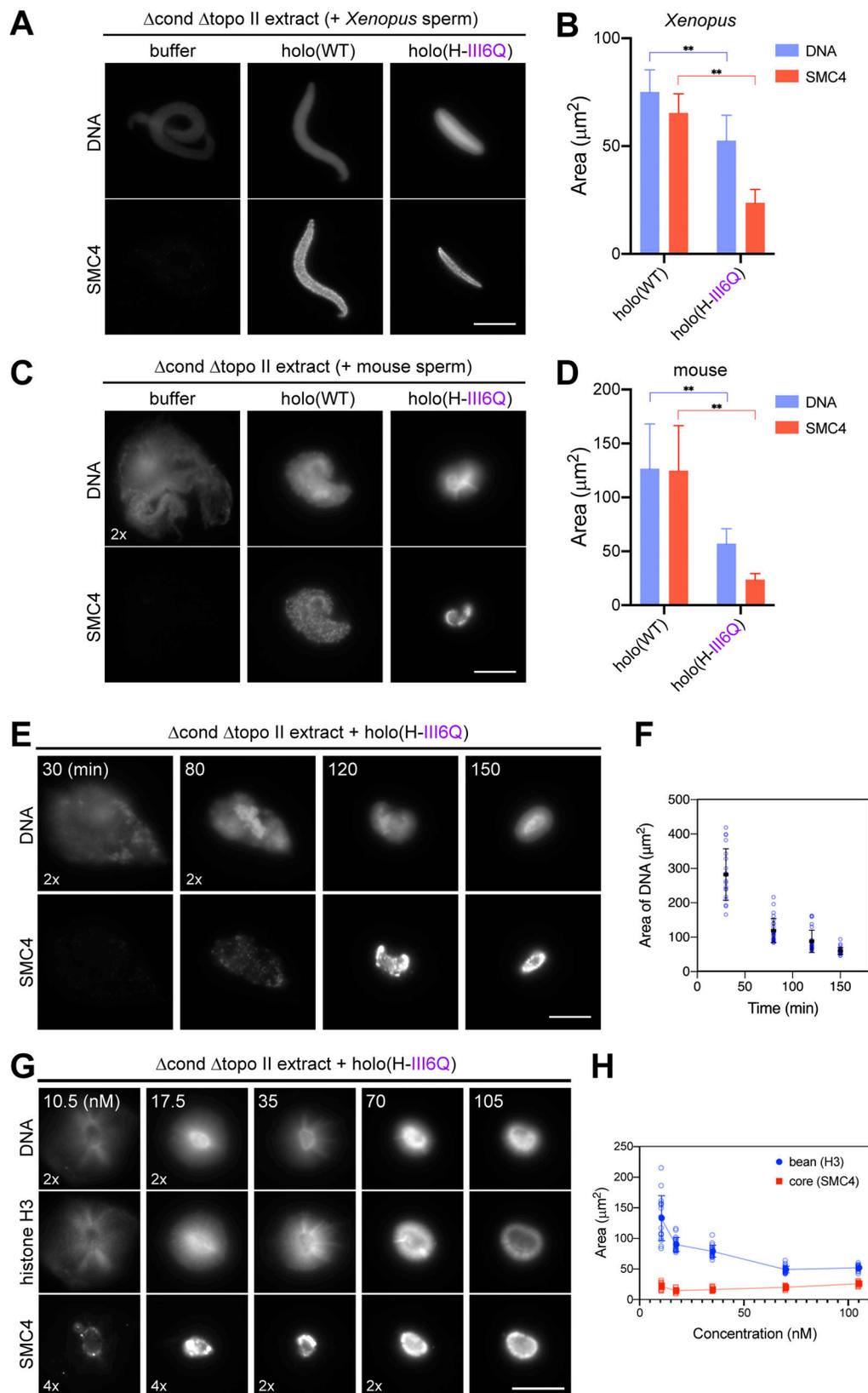
Figure 2. **CAP-H motif III mutant complexes produce "beans" in the absence of topo IIα. (A)** Topo II–depleted add-back assay. *Xenopus* sperm nuclei were incubated with extracts depleted of both condensins and topo IIα (Δcond Δtopo II) that had been supplemented with a control buffer, holo(WT), or holo-(H-III6Q). After 120 min, the reaction mixtures were fixed and labeled with an antibody against SMC4. DNA was counterstained with DAPI. The data from a single representative experiment out of three repeats are shown. Scale bar, 10 μm. **(B)** Quantification of DNA-positive (shown in blue) and SMC4-positive (shown in red) areas in the chromatin structures shown in A. The mean and SD are shown (*n* = 30, 27 from left to right). **, P < 0.01 by a two-tailed Mann-

Kinoshita et al.
Chromosome shaping by condensin I

Journal of Cell Biology   5 of 17
https://doi.org/10.1083/jcb.202109016

Whitney *U* test. **(C)** Topo II–depleted add-back assay. Mouse sperm nuclei were incubated with the same set of extracts as described in A for 150 min and analyzed as above. A different relative exposure time (2x) was used where indicated. The data from a single representative experiment out of three repeats are shown. Scale bar, 10 µm. **(D)** Quantification of DNA-positive (shown in blue) and SMC4-positive (shown in red) areas in the chromatin structures shown in C. The mean and SD are shown (*n* = 25, 34 from left to right). **, P < 0.01 by a two-tailed Mann-Whitney *U* test. **(E)** Time course of bean formation. Mouse sperm nuclei were incubated with a Δcond Δtopo II extract that had been supplemented with holo(H-III6Q). Aliquots were taken at the time points indicated, fixed, and analyzed as in C. Different relative exposure times were used wherever indicated (2x). Scale bar, 10 µm. **(F)** Quantification of DNA-positive areas in the chromatin structures shown in E. The mean and SD are shown (*n* = 20, 26, 26, and 29 from 30 to 150 min). **(G)** Titration experiment. Mouse sperm nuclei were incubated with Δcond Δtopo II extracts that had been supplemented with the indicated concentrations of holo(H-III6Q). After 150 min, the reaction mixtures were fixed and labeled with antibodies against histone H3 and SMC4. DNA was counterstained with DAPI. Different relative exposure times were used wherever indicated (2x or 4x). Scale bar, 10 µm. **(H)** Quantification of histone H3-positive (bean, shown in blue) and SMC4-positive (core, shown in red) areas in the structures shown in G. The mean and SD are shown (*n* = 17, 19, 20, 25, and 19 from 10.5 to 105 nM).

form a bean, whereas neither ΔD2(H-III6Q) nor ΔD2ΔG(H-III6Q) formed beans (Fig. 4, A, C, and D), indicating that the bean phenotype depends on CAP-D2 but not on CAP-G.

We then repeated the same set of experiments in the absence of the H-III6Q mutations. To our surprise, it was found that ΔG(WT), but not ΔD2(WT) or ΔD2ΔG(WT), formed beans (Fig. 4 B). The character of the beans produced by ΔG(WT) was very similar to that produced by ΔG(H-III6Q) (Fig. 4, C and D). Thus, the loss of CAP-G makes condensin I competent to form beans, regardless of the presence or absence of the H-III6Q mutations. The formation of a bean by ΔG(WT) was also dose dependent (Fig. S3, A and B), and subsequent addition of topo IIα converted the ΔG(WT)-induced beans into clusters of individualized chromosomes with thin axes (Fig. S3, C–E). These results demonstrated that, like holo(H-III6Q), ΔG(WT) has the ability to form a bean in a CAP-D2–dependent manner.

A contact between CAP-D2 and SMC4 is essential for proper chromosome assembly and shaping

We next wished to understand which domains of CAP-D2 are essential for bean formation. CAP-D2 has ~21–22 units of HEAT repeats along nearly its entire length (Yoshimura and Hirano, 2016; Hassler et al., 2019), which is followed by an intrinsically disordered region at its C terminus (C-tail; Fig. 5 A). A previous structural study had identified a helical domain, called "proboscis," that is located between HEAT 8 and 9 (Hassler et al., 2019). The same study also reported an unanticipated contact between the KG-loop of CAP-D2 (located between HEAT 18 and 19) and the W-loop conserved in the head domain of SMC4. We designed truncation mutations that delete the C-tail (D2-ΔC92) or proboscis (D2-Δprb453-911) and also introduced substitution mutations into the KG-loop (D2-KG mut; Fig. S4 A) that had been shown to impair the D2-SMC4 contact (Hassler et al., 2019). ΔG subcomplexes harboring these CAP-D2 mutations were prepared and tested for their ability to form beans in the topo II–depleted add-back assay. We found that both ΔG(D2-ΔC92) and ΔG(D2-Δprb453-911) could form beans (Fig. 5, B and C). Although the size of a bean formed by the latter was larger than that produced by ΔG(WT), SMC4 signals were still concentrated in the small core. In contrast to the two truncation mutant complexes, ΔG(D2-KG mut) failed to form a bean. SMC4 signals were no longer concentrated in the central cores and were diffused throughout the chromatin masses.

We next prepared a ΔG subcomplex harboring a mutation in the W-loop of SMC4 (SMC4-W1183A; Fig. S4 A) that had been

shown to impair the D2-SMC4 contact (Hassler et al., 2019), and we found that ΔG(SMC4-W1183A) displayed a defective phenotype similar to that displayed by ΔG(D2-KG mut) in the same assay (Fig. 5, D and E). We then wondered what would happen if the two mutant complexes were mixed together, with a hypothesis in our mind that the D2-SMC4 contact could be made not only within a complex but also between different complexes (Fig. S4 A). Remarkably, it was found that a mixture of ΔG(D2-KG mut) and ΔG(SMC4-W1183A) exhibited a partial bean phenotype with SMC4 signals concentrated in the central part of DNA-positive areas.

We then repeated the same set of experiments in the context of holocomplexes in the presence of topo IIα (Fig. 5 F). Each of holo(D2-KG mut) and holo(SMC4-W1183A) exhibited a poor ability to assemble individualized chromosomes, and only faint and diffuse signals of SMC4 were detectable on the chromatin. We found, however, that a mixture of holo(D2-KG mut) and holo(SMC4-W1183A) produced chromosomes with better progression of individualization and with a more axial enrichment of SMC4 and topo IIα signals than when each of the mutant complexes was added alone. Accordingly, the compaction index (as defined by the average DNA intensity per unit area; Shintomi and Hirano, 2021) of these structures was restored to a level comparable to that of the control chromosomes produced by holo(WT) (Fig. 5 G), although the former is slightly thicker than the latter (Fig. 5 H). These results suggested that the two mutant complexes, when mixed together, cooperate to support mitotic chromosome assembly. Implications of these observations are discussed in the Discussion section. Note that although the partial rescue observed in these mixing experiments could in theory be caused by subunit exchange between the two different input complexes, we confirmed that such exchange barely occurred in egg extracts under our experimental condition (Fig. S4, B and C).

Loop extrusion activities of the condensin I mutant complexes

Recent demonstrations of loop extrusion activities associated with condensin complexes in vitro (Ganji et al., 2018; Kong et al., 2020) prompted us to test to what extent our mutant complexes retain such activities. To this end, we prepared a panel of fluorescently labeled complexes and performed a single-molecule loop extrusion assay using U-shaped DNAs as a substrate (Sakata et al., 2021). We found that, in our setup, holo(WT) converted ~50% of the U-shaped DNAs into loops in an ATP-dependent manner (Fig. 6 A). Importantly, the vast majority of
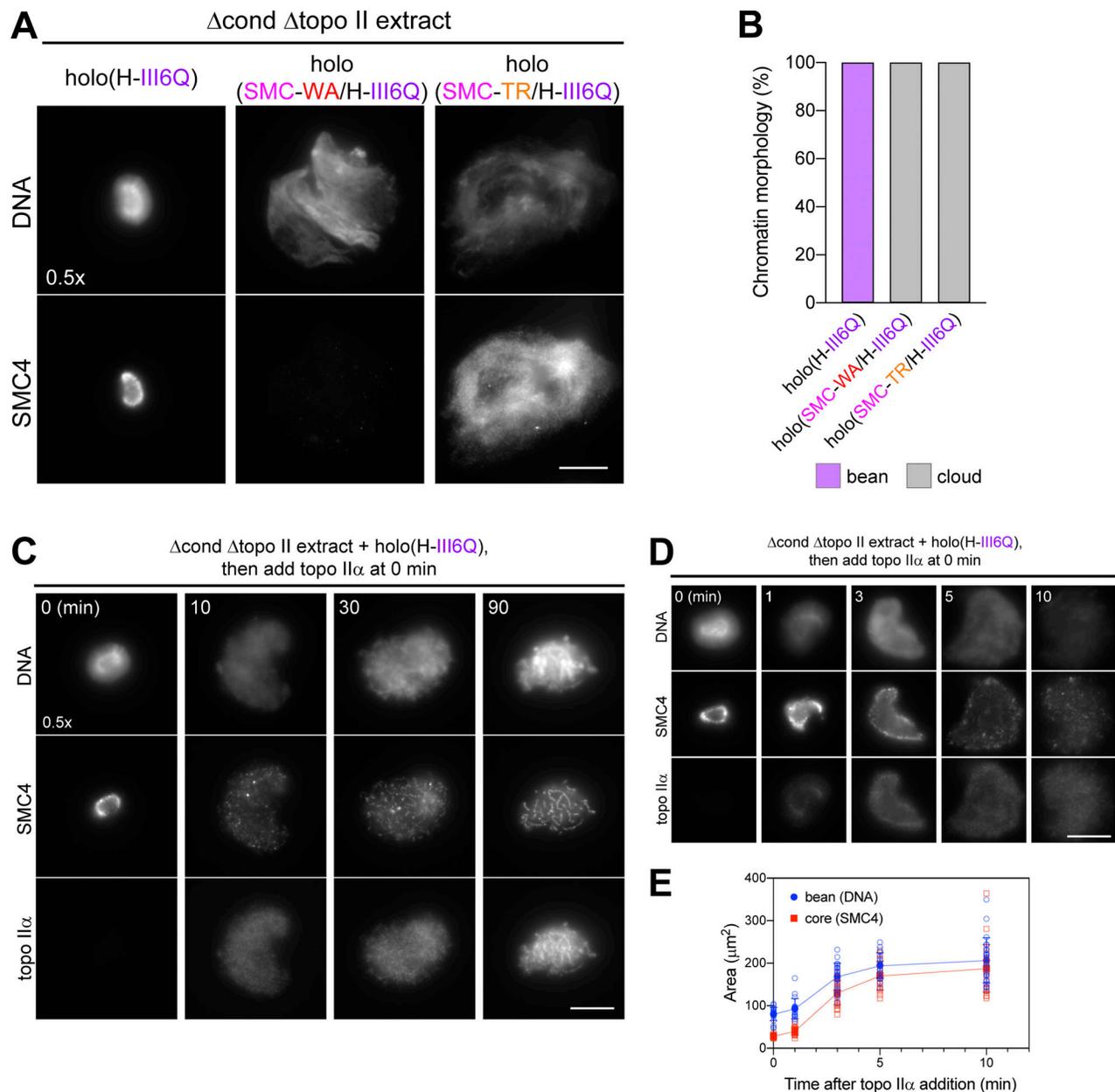
Figure 3. **The bean phenotype depends on the SMC ATPase cycle and can be reversed by subsequent addition of topo IIα. (A)** Topo II–depleted add-back assay. Mouse sperm nuclei were incubated with Δcond Δtopo II extracts that had been supplemented with holo(H-III6Q), holo(SMC-WA/H-III6Q), or holo(SMC-TR/H-III6Q). After 150 min, the reaction mixtures were fixed and labeled with an antibody against SMC4. DNA was counterstained with DAPI. A different relative exposure time (0.5x) was used where indicated. Scale bar, 10 μm. **(B)** Chromosome morphology as judged by the DAPI-stained images shown in A. In each reaction, the morphology of the final products was highly homogeneous, displaying either "bean" or "cloud" morphology (n = 28, 13, and 14 from left to right). **(C)** Add-back of topo IIα after bean formation. Mouse sperm nuclei were mixed with a Δcond Δtopo II extract that had been supplemented with holo(H-III6Q) and incubated for 150 min to assemble beans. A Δcond extract (containing native *Xenopus* topo IIα) that had been supplemented with holo(H-III6Q) was then added at time 0 min (Fig. S2 C). Aliquots were taken at the time points indicated, fixed, and labeled with antibodies against SMC4 and topo IIα. DNA was counterstained with DAPI. A different relative exposure time (0.5x) was used where indicated. Scale bar, 10 μm. **(D)** Add-back of topo IIα after bean formation. The same assembly mixture was set up as in C, but aliquots were taken at the earlier time points indicated and analyzed as above. Scale bar, 10 μm. **(E)** Quantification of DNA-positive (bean, shown in blue) and SMC4-positive (core, shown in red) areas in the structures shown in D. The mean and SD are shown (n = 21, 19, 23, 18, and 23 from 0 to 10 min).

labeled holo(WT), which most likely corresponded to single complexes, was found at the base of those loops (Fig. 6 B; and Fig. S5, A–C). In the first set of experiments, we tested the two mutant complexes (holo[H-III6Q] and ΔG[WT]) that displayed the bean phenotype in the absence of topo IIα. It was found that

holo(H-III6Q) supported loop formation at a lower frequency than holo(WT), whereas ΔG(WT), although detectable on the DNA substrate, barely supported loop formation (Fig. 6 C and Fig. S5 D). Despite their difference in the frequency of loop formation, the rate of loop extrusion and the size of formed
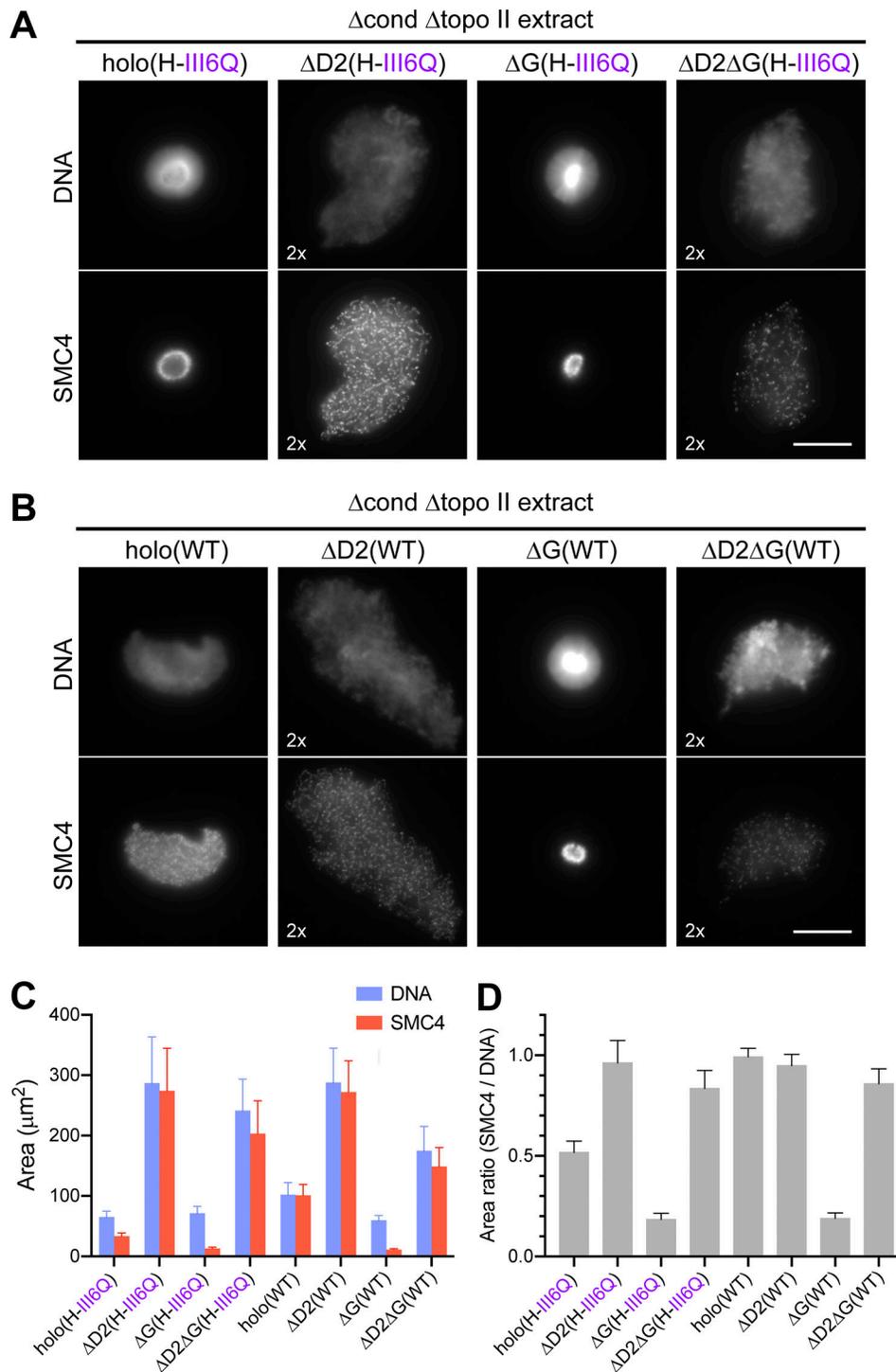
Figure 4. **The bean phenotype depends on CAP-D2 but not on CAP-G. (A)** Topo II–depleted add-back assay using subcomplexes harboring the H-III6Q mutations. Mouse sperm nuclei were incubated with Δcond Δtopo II extracts that had been supplemented with holo(H-III6Q), ΔD2(H-III6Q), ΔG(H-III6Q), or ΔD2ΔG(H-III6Q). After 150 min, the reaction mixtures were fixed and labeled with an antibody against SMC4. DNA was counterstained with DAPI. Different relative exposure times were used wherever indicated (2x). Scale bar, 10 μm. **(B)** Topo II–depleted add-back assay using subcomplexes without the H-III6Q mutations. Mouse sperm nuclei were incubated with Δcond Δtopo II extracts that had been supplemented with holo(WT), ΔD2(WT), ΔG(WT), or ΔD2ΔG(WT) for 150 min and analyzed as in A. Different relative exposure times were used wherever indicated (2x). Scale bar, 10 μm. **(C)** Quantification of DNA-positive (bean, shown in blue) and SMC4-positive (core, shown in red) areas in the structures shown in A and B. The mean and SD are shown (n = 28, 26, 30, 22, 29, 29, 30, and 27 from left to right). **(D)** Comparison of the ratio of SMC4-positive to DNA-positive areas measured in C. The mean and SD are shown.
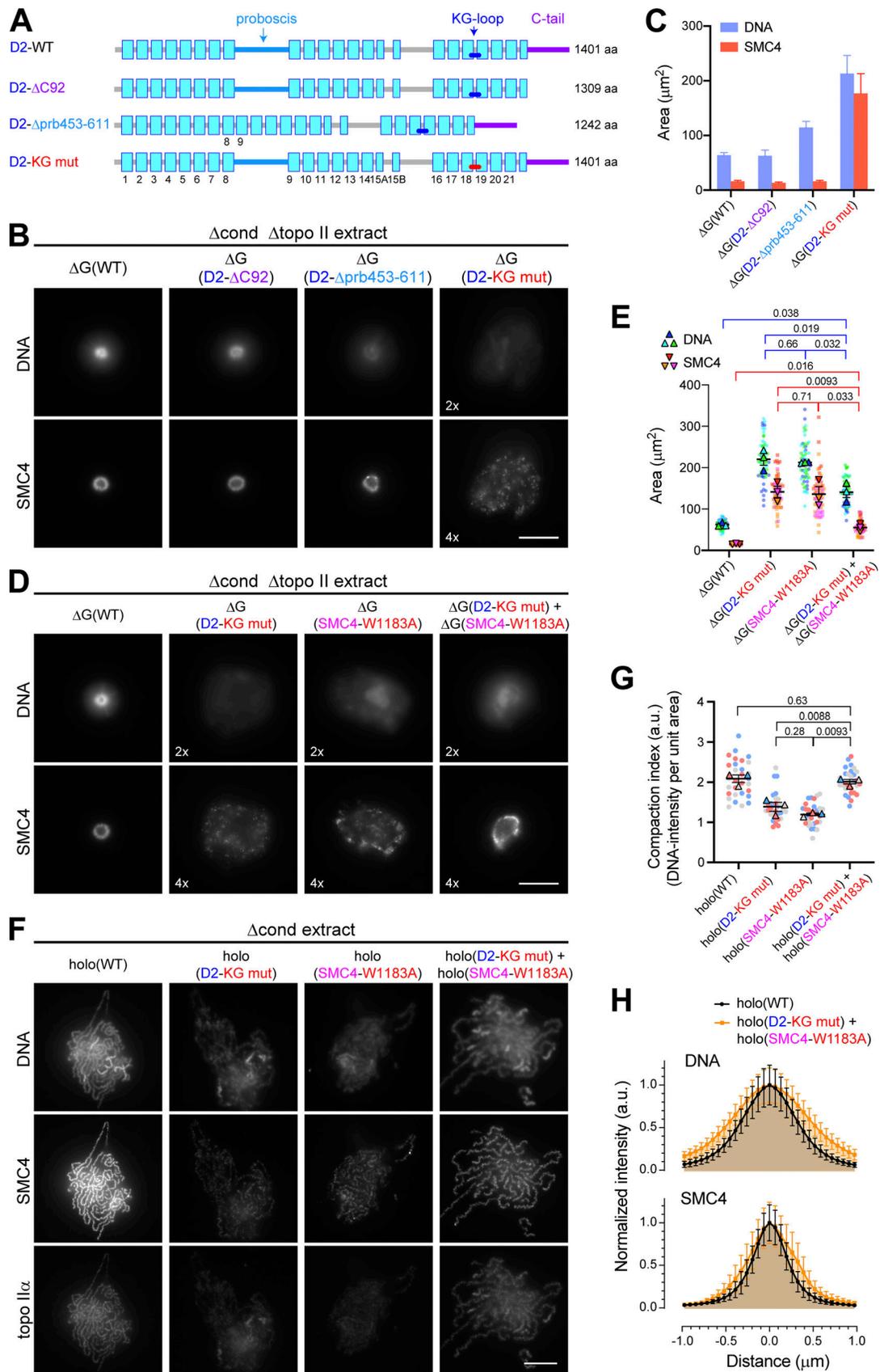
Figure 5. **A contact between CAP-D2 and SMC4 is essential for proper chromosome assembly and shaping. (A)** Mutagenesis of the CAP-D2 subunit. The light blue box indicates a HEAT repeat unit. The D2-ΔC92 mutant lacks a 92-aa-long C-terminal tail of CAP-D2, which is intrinsically disordered. The

D2-Δprb453-611 lacks a helical insertion domain, called "proboscis," that is located between the HEAT repeat motifs 8 and 9. The D2-KG mut has substitution mutations (from KVKGQV to DSDGDS) in the KG-loop that is located between the HEAT repeat motifs 18 and 19 (see also Fig. S4 A). **(B)** Topo II–depleted add-back assay using ΔG subcomplexes harboring the CAP-D2 mutations. Mouse sperm nuclei were incubated with Δcond Δtopo II extracts that had been supplemented with ΔG(WT), ΔG(D2-ΔC92), ΔG(D2-Δprb453-611), or ΔG(D2-KG mut). After 150 min, the reaction mixtures were fixed and labeled with an antibody against SMC4. DNA was counterstained with DAPI. Different relative exposure times were used wherever indicated (2x or 4x). Scale bar, 10 µm. **(C)** Quantification of DNA-positive (bean, shown in blue) and SMC4-positive (core, shown in red) areas in the structures shown in B. The mean and SD are shown (n = 34, 28, 24, and 27 from left to right). **(D)** Topo II–depleted add-back assay using ΔG subcomplexes harboring D2-KG mut or SMC4-W1183A. Mouse sperm nuclei were incubated with Δcond Δtopo II extracts that had been supplemented with ΔG(WT), ΔG(D2-KG mut), or ΔG(SMC4-W1183A) at a concentration of 35 nM, or a mixture of ΔG(D2-KG mut) and ΔG(SMC4-W1183A) at a concentration of 17.5 nM each. After 150 min, the reaction mixtures were fixed and labeled with an antibody against SMC4. DNA was counterstained with DAPI. Different relative exposure times were used wherever indicated (2x or 4x). The data from a single representative experiment out of three replicates are shown. Scale bar, 10 µm. **(E)** Quantification of DNA-positive and SMC4-positive areas in the structures shown in D. Three biological replicates are color coded. For DNA-positive areas, data points are shown by the dots (blue, cyan, or green), and averages from individual experiments are shown by the triangles with the corresponding colors. For SMC4-positive areas, data points are shown by the dots (red, orange, or magenta), and averages from individual experiments are shown by the inverted triangles with the corresponding colors. Error bars represent SEM from n = 3 independent experiments, in each of which 20 chromatin masses were analyzed. The P values were assessed by a paired two-tailed t test. **(F)** Add-back assay using holocomplexes harboring D2-KG mut or SMC4-W1183A. Mouse sperm nuclei were incubated with Δcond extracts that had been supplemented with holo(WT), holo(D2-KG mut), or holo(SMC4-W1183A) at a concentration of 35 nM, or a mixture of holo(D2-KG mut) and holo(SMC4-W1183A) at a concentration of 17.5 nM each. After 150 min, the reaction mixtures were fixed and labeled with antibodies against SMC4 and topo IIα. DNA was counterstained with DAPI. The data from a single representative experiment out of three replicates are shown. Scale bar, 10 µm. **(G)** Quantification of the ratio of DNA intensity to DNA-positive area in the structures shown in F. Three biological replicates are color coded. Data points are shown by the dots (blue, red, or gray), and averages from individual experiments are shown by the triangles with the corresponding colors. Error bars represent SEM from n = 3 independent experiments, in each of which 10 clusters of chromosomes were analyzed. The P values were assessed by a paired two-tailed t test. **(H)** Line profiles of chromosomes assembled with holo(WT) (black) or a mixture of holo(D2-KG mut) and holo(SMC4-W1183A) (orange) shown in F. The signal intensities of DNA (top) and SMC4 (bottom) were scanned along the lines drawn perpendicular to chromosome axes (n = 20). The mean and SD of 20 lines were plotted as normalized intensities (a.u.).

loops were indistinguishable between holo(H-III6Q) and holo(WT) (Fig. 6, D and F). A small difference was detectable, however, in the loop duration time between the two complexes (Fig. 6 E), suggesting that DNA loops formed by holo(H-III6Q) were less stable than those formed by holo(WT).

In the second set of experiments, we tested the three mutant complexes (holo[D2-KG mut], holo[SMC4-W1183A], and ΔD2 [WT]) that did not display the bean phenotype in the absence of topo IIα. It was found that both of holo(D2-KG mut) and holo(SMC4-W1183A) could support loop formation, albeit at a lower frequency than holo(WT), whereas ΔD2(WT) hardly formed DNA loops (Fig. 6 G). Despite the lower frequencies of loop formation, once loops are formed, notable differences were not observed in the three parameters among holo(WT), holo(D2-KG mut), and holo(SMC4-W1183A) (Fig. 6, H–J). Taken together, these results demonstrated that the loop extrusion activities of the mutant complexes cannot explain the contrasting defective phenotypes they exhibit in the add-back assays.

Discussion

Xenopus and mouse sperm nuclei respond differently to various perturbations

A previous work from our laboratory had reported that the two HEAT subunits, CAP-D2 and CAP-G, have antagonistic effects on the dynamic assembly of mitotic chromosome axes (Kinoshita et al., 2015). One of the initial motivations behind the present study was to address the function of the kleisin subunit CAP-H with a major focus on a conserved motif (motif III) present in its middle region. To this end, we designed and prepared a mutant holocomplex harboring motif III mutations, holo(H-III6Q). Although holo(H-III6Q) failed to individualize chromosomes when *Xenopus* sperm nuclei were used as a substrate, the same mutant complex could assemble individualized chromosomes with confined axes when mouse sperm nuclei were used (Fig. 1, B–E). We had noticed before that topo IIα depletion causes different degrees of individualization defects between the two substrates (Hirano and Mitchison, 1993; Shintomi et al., 2017). These observations allow us to speculate that chromosomal DNAs within *Xenopus* sperm nuclei are entangled with each other more heavily than those within mouse sperm nuclei. Nevertheless, when the add-back assay was set up in the absence of topo IIα, holo(H-III6Q) now exhibited qualitatively similar morphological defects in both substrates, producing more compact structures than holo(WT) with condensin-positive substructures in their central part (Fig. 2, A–D).

Following the early set of our observations described above, a structural study reported that CAP-G/Ycg1 and the motif III of CAP-H/Brn1 constitute a part of the unique DNA binding domain named the "safety belt" (Kschonsak et al., 2017). The H-III6Q mutations are similar but not identical to one of the safety belt mutations (Brn1-ϕD) reported by Kschonsak et al. (2017). We therefore prepared an additional pair of safety belt mutant complexes, holo(H-III4D) and holo(H-BC1/2D), and found that both complexes exhibit defective phenotypes similar to those of holo(H-III6Q) under various conditions (Fig. S1). We speculate that these mutations in CAP-H partially compromise its functional interactions with CAP-G, which in turn causes imbalance in action between CAP-D2 and CAP-G (see below). It is important to note that all of these mutant complexes, at least in part, retain their ability to associate with chromosomes in our functional assays and to assemble confined axial structures positive for condensin subunits. Thus, condensin I has a loading mechanism that is independent of the proposed safety belt (for additional discussion, see Hara et al., 2019).
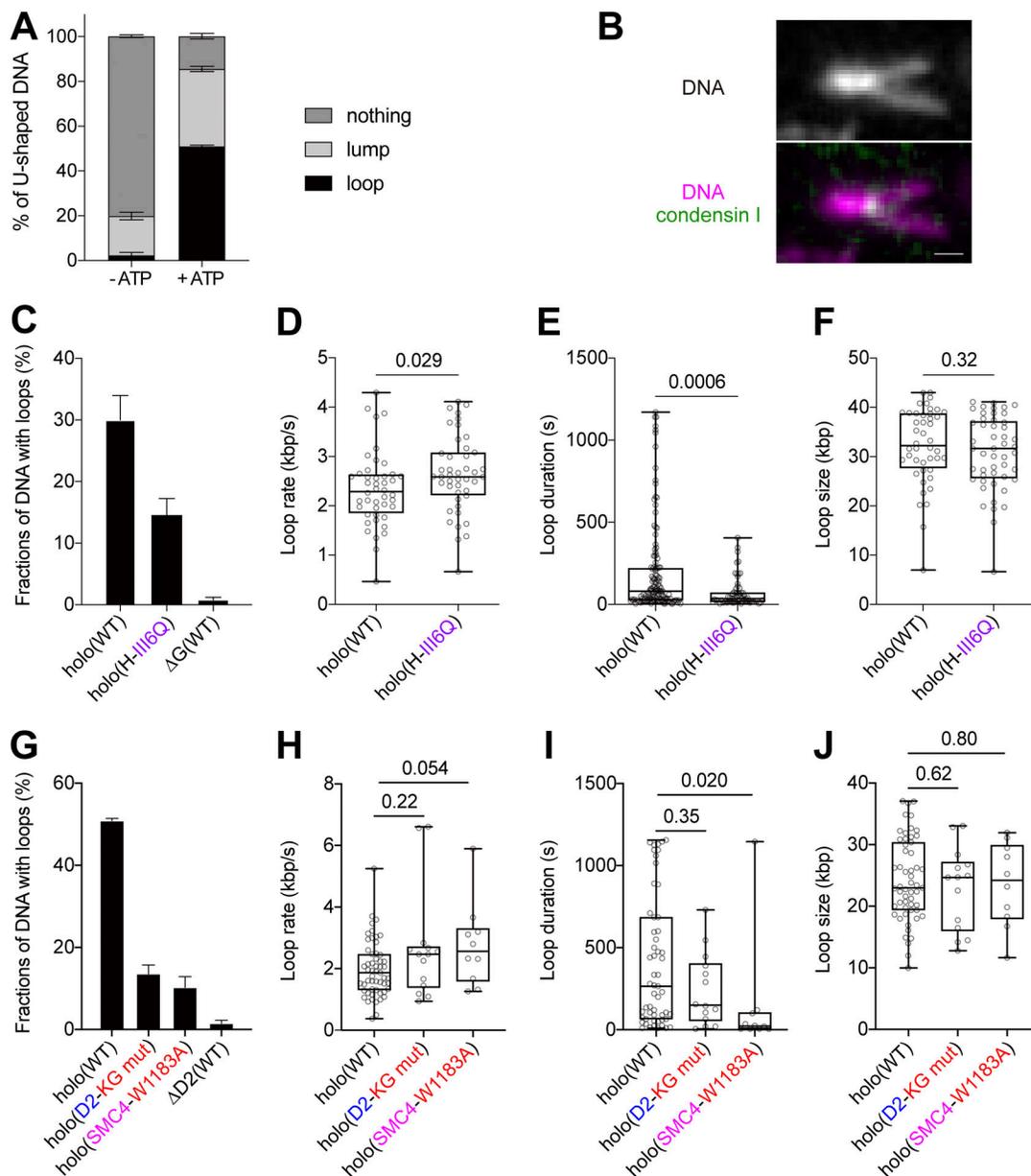
Figure 6. **Loop extrusion activities of the condensin I mutant complexes. (A)** Frequency of DNA loop formation by holo(WT) in the presence or absence of ATP (*n* = 3; ≥42 DNAs per condition; mean ± SEM). A nonloop compact structure of DNA observed regardless of the presence or absence of ATP was categorized as the "lump." **(B)** Still image of DNA loop formed by holo(WT). Scale bar, 1 µm. **(C)** Frequency of DNA loop formation by holo(WT), holo(H-III6Q), or ΔG(WT) (*n* = 5; ≥61 DNAs per condition; mean ± SEM). **(D)** Loop extrusion rate by holo(WT) or holo(H-III6Q) (from five independent experiments; *n* = 44, 44 from left to right). The P values were assessed by a two-tailed Mann-Whitney *U* test. **(E)** Duration time to maintain DNA loops by holo(WT) or holo(H-III6Q) (from five independent experiments; *n* = 135, 62 from left to right). The P values were assessed by a two-tailed Mann-Whitney *U* test. The median values for holo(WT) and holo(H-III6Q) are 80 s and 35 s, respectively. **(F)** Loop size produced by holo(WT) or holo(H-III6Q) (from five independent experiments; *n* = 44, 49 from left to right). The P values were assessed by a two-tailed Mann-Whitney *U* test. **(G)** Frequency of DNA loop formation by holo(WT), holo(D2-KG mut), holo(SMC4-W1183A), or ΔD2(WT) (*n* = 3; ≥43 DNAs per condition; mean ± SEM). **(H)** Loop extrusion rate by holo(WT), holo(D2-KG mut), or holo(SMC4-W1183A) (from three independent experiments; *n* = 55, 14, and 10 from left to right). The P values were assessed by a two-tailed Mann-Whitney *U* test. **(I)** Duration time to maintain DNA loops by holo(WT), holo(D2-KG mut), or holo(SMC4-W1183A) (from three independent experiments, *n* = 55, 14, and 10 from left to right). The P values were assessed by a two-tailed Mann-Whitney *U* test. **(J)** Loop size produced by holo(WT), holo(D2-KG mut), or holo(SMC4-W1183A) (from three independent experiments; *n* = 55, 14, and 10 from left to right). The P values were assessed by a two-tailed Mann-Whitney *U* test.

The class I and class II mutations cause contrasting defective phenotypes in add-back assays

Chromosomal DNAs within sperm nuclei are entangled with each other, and topo IIα–mediated disentanglement acts as an essential prerequisite for individualizing chromosomes (Hirano and Mitchison, 1993; Shintomi et al., 2015; Shintomi and Hirano, 2021). The actions of topo IIα and condensin I are interdependent with each other, however: Condensin I–mediated loop extrusion directs topo IIα to resolve entangled DNAs, whereas the resulting liberated DNAs act as a suitable substrate for

condensin I's action (Fig. 7 A, right, top). In the absence of topo IIα, the extrusion-dependent processes would be restricted, and condensin I would be stuck on the entangled DNAs. Under this condition, holo(WT) distributes uniformly on the entangled chromatin masses, whereas holo(H-III6Q) is concentrated in the core of the bean (Fig. 7 A, right, bottom). The bean is not a mere aggregate of the mutant complexes, because its formation requires a functional SMC ATPase activity and because it can be reversed by subsequent addition of topo IIα (Fig. 3). CAP-D2, but not CAP-G, is essential for bean formation, and ΔG(WT) produces a bean even without the H-III6Q mutations (Fig. 4 and Fig. S3). In the following discussion, we refer to the above-mentioned set of mutations (H-III6Q, H-III4D, and H-BC1/2D), along with the deletion of CAP-G, as the class I mutations. In the presence of topo IIα, holocomplexes harboring the class I substitution mutations produce confined axes, whereas ΔG(WT) produces much thinner abnormal axes (Kinoshita et al., 2015; see also Fig. S3 C). In the absence of topo IIα, all class I mutation–containing complexes induce hypercompaction of DNA to form beans. Thus, the central axis of mitotic chromosomes and the core of beans share many characteristics: Both contain densely packed, possibly entangled, DNAs where condensin I is enriched. We anticipate that studying the molecular mechanism of bean formation will provide a vital clue to increase our understanding of the molecular mechanism of chromosome axis assembly.

Deletion of the CAP-D2 C-tail or proboscis had little effect on ΔG-mediated bean formation in the absence of topo IIα (Fig. 5, B and C). However, mutations in the CAP-D2 KG-loop (D2-KG mut) or the SMC4 W-loop (SMC4-W1183A) canceled ΔG-mediated bean formation, indicating that the D2-SMC4 contact reported by Hassler et al. (2019) is essential for bean formation (Fig. 5, D and E). In the presence of topo IIα, holo(D2-KG mut) and holo(SMC4-W1183A) produced poorly organized chromosomes with diffuse axes, a defective phenotype that contrasts with those caused by the holocomplexes harboring the class I mutations (Fig. 5, F and G). In the following discussion, we refer to the two substitution mutations (D2-KG mut and SMC4-W1183A), along with the deletion of D2, as the class II mutations.

Loop extrusion activities of the mutant complexes cannot explain the chromosomal defects they exhibit in add-back assays

Recent single-molecule analyses have demonstrated that budding yeast condensin, as well as human condensins I and II, exhibit loop extrusion activities in vitro (Ganji et al., 2018; Kong et al., 2020). By setting up a similar single-molecule assay, we found that holo(WT) exhibits an ATP-dependent loop extrusion activity (Fig. 6). Both ΔG(WT) and ΔD2(WT) barely formed DNA loops, suggesting that both HEAT subunits, CAP-D2 and CAP-G, are essential for loop extrusion. Mutant complexes harboring the class I or II substitution mutations formed DNA loops at lower frequencies than holo(WT). Once loops were formed, however, big differences were not detectable among the mutant complexes in other parameters, including loop extrusion rates. It should be added that loop extrusion activities of budding yeast mutant complexes similar to our holo(H-III6Q) and ΔG(WT)

were measured before (Ganji et al., 2018; Ryu et al., 2020) and that our present results are largely consistent with those published (including the interpretation that the H-III6Q mutations cause "slippage" during loop extrusion). Thus, the contrasting defective phenotypes caused by the class I and class II mutations in the add-back assays cannot be explained by loop extrusion activities of the corresponding mutant complexes. Taking all these results together, we suggest that, as opposed to the original proposal (Goloborodko et al., 2016b), the loop extrusion mechanism alone may not be sufficient to properly assemble and shape mitotic chromosomes and that a loop extrusion–independent mechanism also contributes to these processes.

Condensin–condensin interactions underlie mitotic chromosome assembly and shaping

What mechanism(s), besides loop extrusion, might contribute to chromosome assembly and shaping? One possibility is a diffusion capture mechanism (Cheng et al., 2015; Gerguri et al., 2021), whereas another possibility is a mechanism involving condensin–condensin interactions (Sakai et al., 2018). Although the possibility of condensin–condensin interactions has been suggested before (Gerguri et al., 2021; Keenholtz et al., 2017; Yoshimura and Hirano, 2016), no direct evidence has been available to date. Here we hypothesize that the D2-SMC4 contact identified by Hassler et al. (2019) could occur not only within individual complexes but also between different complexes (Fig. 7 B), thereby constituting part of the mechanism that facilitates and/or stabilizes the condensin–condensin interactions. It should be stressed that such interactions would occur only under crowded conditions. In the presence of topo IIα, disentanglement of chromatin fibers ensures that condensin–condensin interactions occur only in cis (within individual chromosomes) to form central axes at a late stage of chromosome assembly (Fig. 7 A). In the absence of topo IIα, chromatin fibers stay entangled, allowing the condensin–condensin interactions to occur also in trans (between different chromosomes), leading to the formation of entangled masses or beans. Consistent with this notion, the D2-SMC4 contact interfaces are intact in holo(WT) (Fig. 7 C, WT) and the complexes harboring the class I mutations (Fig. 7 C, class I), but they are impaired or missing in those harboring the class II mutations (Fig. 7 C, class II). We reason that the flip-flop mechanism recently proposed based on cryo-EM structures (Lee et al., 2020; Fig. 7 B, left and center) provides a mechanistic explanation for the antagonistic actions of CAP-D2 and CAP-G reported before (Kinoshita et al., 2015). In holo(WT), active loop extrusion brings about steric repulsion between the expanding loops (Goloborodko et al., 2016a), which in turn counterbalances the D2-dependent condensin–condensin interactions (Fig. 7 A). In the mutant complexes harboring the class I mutations, such counteractions decrease, and the condensin–condensin interactions dominate, thereby resulting in the hypercompaction phenotypes (i.e., confined axis formation in the presence of topo IIα and core formation in its absence).

Further support for the hypothesis came from the mixing experiment: We found that holo(SMC4-W1183A) and holo(D2-KG mut), when mixed together, partially restored the defects exhibited by each of the single-mutant complexes (Fig. 5, D–H).
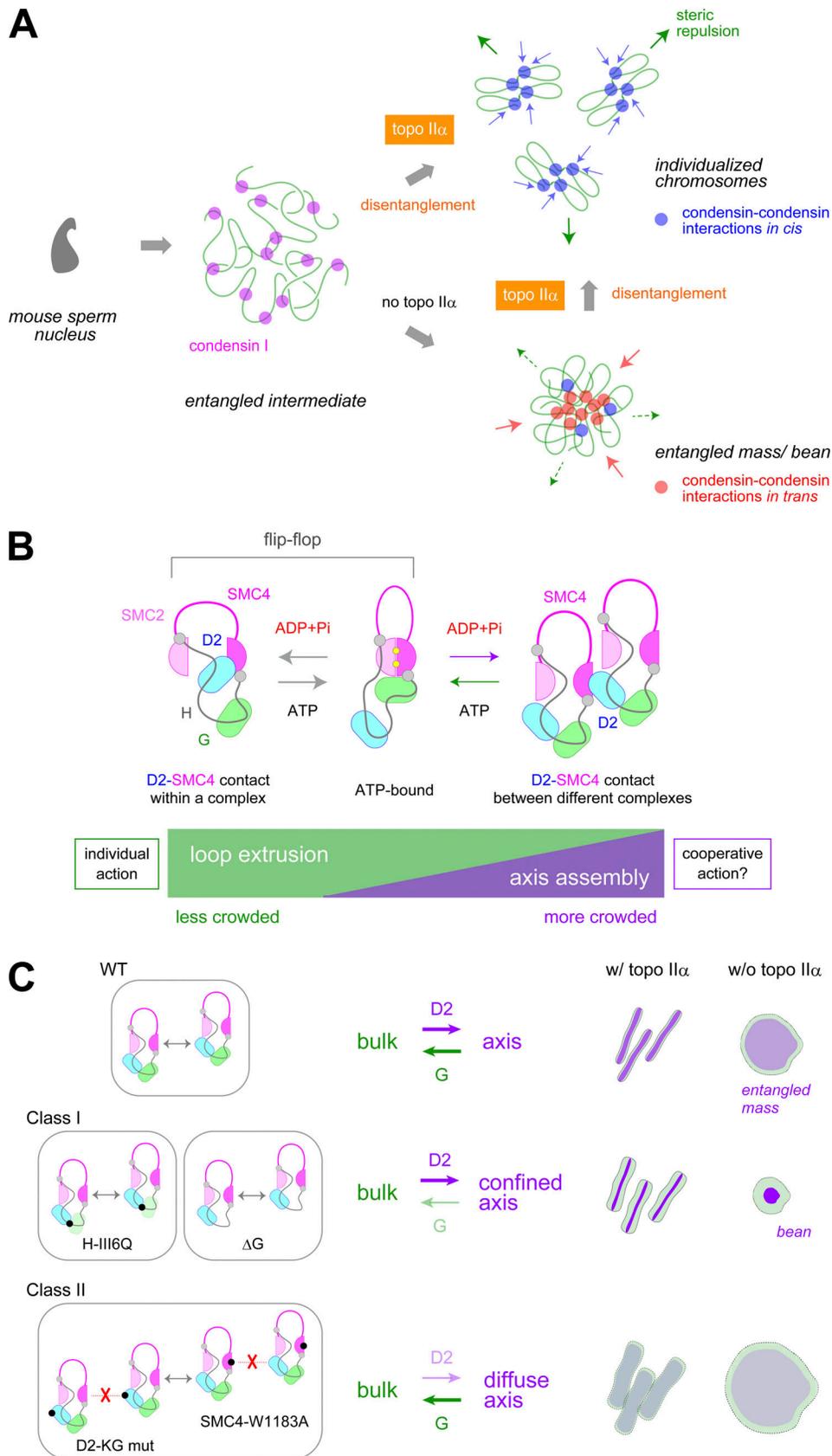
Figure 7. **Models for condensin I–mediated chromosome assembly and shaping. (A)** Chromosomal DNAs are entangled with each other within the mouse sperm nucleus. Upon incubation with a *Xenopus* egg extract, the nucleus rapidly swells following protamine release, and condensin I binds to entangled chromatin fibers. Topo IIα collaborates with condensin I to disentangle chromatin fibers, ensuring that the condensin–condensin interactions occur only in cis

Kinoshita et al.
Chromosome shaping by condensin I

Journal of Cell Biology   13 of 17
https://doi.org/10.1083/jcb.202109016

(within individual chromosomes). Steric repulsion between the loops, caused by condensin-mediated loop extrusion, further facilitates the individualization process. In the absence of topo IIα, no disentanglement is catalyzed, and the condensin–condensin interactions occur not only in cis but also in trans (between different chromosomes), producing an entangled chromatin mass or a bean. **(B)** According to the flip-flop mechanism proposed by Lee et al. (2020), CAP-G is mobile when CAP-D2 makes a contact with SMC4 in the absence of ATP (left). However, CAP-D2 becomes mobile when the SMC heads are engaged in the presence of ATP (center). This mechanism may underlie ATP-dependent loop extrusion supported by individual condensin complexes. We hypothesize that, under crowded conditions, the D2-SMC4 contact could also occur between different condensin complexes to facilitate chromosome axis assembly (right). **(C)** In the case of the WT holocomplex, balancing acts of the CAP-D2 and CAP-G subunits support the assembly of chromosome axes (Kinoshita et al., 2015). In the case of the mutant complex harboring H-III6Q or ΔG (class I), D2-dependent condensin–condensin interactions dominate over loop extrusion, producing confined axes. In the case of the mutant complex harboring D2-KG mut or SMC4-W1183A (class II), the D2-dependent condensin–condensin interactions are compromised, producing diffuse axes. When the two mutant complexes are mixed together, the interactions are partially restored (inset, gray double arrow), producing nearly normal yet slightly thick chromosomes. In the absence of topo IIα (far right), no individualization occurs, and the WT and mutant complexes behave accordingly to produce entangled masses (or beans) of different sizes.

It is plausible to speculate that this apparent suppression is mediated by interactions between the two mutant complexes through their intact interfaces (Fig. 7 C, class II, gray arrow). The collaborative action of the two mutant complexes postulated here is reminiscent of, if not identical to, interallelic complementation observed for two different alleles of the kleisin subunit of cohesin, which provides evidence for cohesin–cohesin interactions in yeast cells (Eng et al., 2015).

Finally, it should be added that the idea discussed here can readily be applied to condensin II because the sequence corresponding to the CAP-D2 KG-loop is conserved in the CAP-D3 subunit of condensin II (Hassler et al., 2019). In the case of cohesin, different mechanisms could mediate cohesin–cohesin interactions (Eng et al., 2015; Ryu et al., 2021; Xiang and Koshland, 2021). Alternatively, a loop extrusion activity (Davidson et al., 2019; Kim et al., 2019) alone could be sufficient to bring cohesins located at the base of loops together and to form an axis-like structure observed in interphase cells depleted of the cohesin regulator Wapl (Tedeschi et al., 2013). In any case, critically addressing both conservation and variations among different SMC protein complexes will enrich our understanding of this class of highly sophisticated protein machines for genome organization.

Limitations of the present study

We must admit that there is a sizable gap between the two experimental systems used in the present study, namely the morphological assay using crude egg extracts and the loop extrusion assay using purified components. For instance, the former assay faithfully recapitulates mitotic phosphorylation of condensin I and its action on chromatin templates, whereas the latter assay does not. The present study nonetheless provides strong lines of evidence that condensin I is equipped with a previously undescribed activity that contributes to mitotic chromosome assembly and shaping. Exactly how the loop extrusion activity might collaborate with other activities such as condensin–condensin interactions proposed here is a fundamental question to be addressed in the future.

Materials and methods

Protein expression and purification of recombinant condensin I complexes

Condensin subunits were expressed in insect cells using the Bac-to-Bac baculovirus expression system (Thermo Fisher Scientific)

as described previously (Kinoshita et al., 2015) with some modifications. Mouse cDNAs for SMC2 and SMC4 and human cDNAs for CAP-D2, -G, and -H were used to make recombinant baculoviruses, and the resulting holocomplex was composed of two mouse subunits (mSMC2 and mSMC4) and three human subunits (hCAP-D2, hCAP-G, and hCAP-H; Kinoshita et al., 2015). For mutagenesis of SMC4-W1183A, the following primers were used: forward 5′-GAAAAGTGCGAAGAAGATCTTTAA CCT-3′, reverse 5′-TTCTTCGCACTTTTCTTAGGTGGCCG-3′. In early constructs, the H-III6Q mutations were introduced into the plasmid pFH101 using the QuikChange II XL Site-Directed Mutagenesis Kit (Agilent Technologies). The following primers were used for mutagenesis of the H-III6Q mutations: Y417Q Y419Q F420Q, 5′-AAACCTGGAGAACAATCTCAACAAAGTCCT CGGACCATG-3′; W434Q F436Q, 5′-CTGGCCCGGATCACCAGC GCCAAAGGCCTCGACGCA-3′; W428Q, 5′-CGGACCATGTCGATG CAGGCTGGCCCGGATCAC-3′. In more recent constructs, we synthesized codon-optimized cDNAs for the three non-SMC subunits (GeneArt Gene Synthesis Service; Thermo Fisher Scientific) and used them accordingly. Cell lysates were prepared by cotransfecting High Five cells (Thermo Fisher Scientific) with recombinant baculoviruses expressing individual subunits. An early set of holo- and subcomplexes were purified as described previously (Kinoshita et al., 2015), and a recent set of recombinant complexes was purified by two-step column chromatography. In brief, cell lysates were first applied to Glutathione Sepharose 4B beads (Cytiva) to enrich protein complexes containing GST-tagged SMC4 subunits. The beads were then treated with PreScission protease (Cytiva) to cleave the GST tag off, and released fractions were loaded onto a HiTrap Q HP column (Cytiva) that had been equilibrated with binding buffer (40 mM Tris-HCl [pH 7.5], 100 mM NaCl). After the column was washed with the binding buffer, it was developed with a linear gradient of NaCl (100–500 mM). Peak fractions were pooled, concentrated with Amicon Ultra-15 (Merck Millipore), aliquoted, and stored at –80°C.

Antibodies

Primary antibodies used in in the present study were as follows: anti-XSMC4/XCAP-C (in-house identifier AfR8L, affinity-purified rabbit antibody), anti-XSMC2/XCAP-E (AfR9-6, affinity-purified rabbit antibody), anti-XCAP-D2 (AfR16L, affinity-purified rabbit antibody), anti-XCAP-G (AfR11-3L, affinity-purified rabbit antibody; Hirano and Mitchison, 1994; Hirano et al., 1997), anti-XCAP-D3

(AfR196-2L, affinity-purified rabbit antibody), anti-XCAP-H2 (AfR201-4, affinity-purified rabbit antibody; Ono et al., 2003), anti-mSMC4 (AfR326-3L, affinity-purified rabbit antibody; Lee et al., 2011), anti-XSMC3 (AfR48-5L, affinity-purified rabbit antibody; Losada et al., 1998), anti–topo IIα (in-house identifier αC1-6, rabbit anti-serum; Hirano and Mitchison, 1993), anti-histone H3 (CMA301: MABI0301 [RRID AB_1977240]; MBL, mouse antibody), and anti-topo II (AK5: M052-3 [RRID AB_592894]; MBL, mouse antibody). Secondary antibodies used in the present study were as follows: HRP-conjugated anti-rabbit IgG (PI-1000 [RRID AB_2336198], Vector Laboratories, goat antibody), Alexa Fluor 488 anti-rabbit IgG (A-11008 [RRID AB_143165], Thermo Fisher Scientific, goat antibody), Alexa Fluor 568 anti-mouse IgG (A-10037 [RRID AB_2534013], Thermo Fisher Scientific, donkey antibody).

Preparation of *Xenopus* egg extracts and immunodepletions
The high-speed supernatant (HSS) of metaphase-arrested *Xenopus* egg extracts was prepared as described previously (Hirano et al., 1997). Throughout the main text, the HSS of metaphase-arrested *Xenopus* egg extracts is described as an egg extract. Immunodepletion of *Xenopus* condensins I and II from the extracts was performed as described previously (Kinoshita et al., 2015) with some modifications. A first mixture of antibodies containing 12.5 µg of affinity-purified anti-XCAP-D2, 6.25 µg each of affinity-purified anti-XSMC4 and anti-XSMC2, was coupled to 100 µl of Dynabeads Protein A (Thermo Fisher Scientific), whereas a second mixture of antibodies containing 6.25 µg each of affinity-purified anti-XCAP-D3, anti-XSMC2, anti-XCAP-G, and anti-XCAP-H2 was coupled to another 100 µl of Dynabeads Protein A. 100 µl of an extract were incubated with the first pool of beads at 4°C for 30 min and then incubated with the second pool of beads for another 30 min. The supernatant after the two successive rounds of depletion was used as a condensin-depleted extract (Δcond extract). For immunodepletion of topo IIα, 50 µl of anti–topo IIα serum were coupled to 200 µl of the Dynabeads Protein A, and the resulting antibody-coupled beads were washed twice with PBS-TX (PBS, 0.1% Triton X-100) and twice with XBE2 (10 mM Hepes-KOH [pH 7.7], 100 mM KCl, 2 mM MgCl$_2$, 0.1 mM CaCl$_2$, 5 mM EGTA, and 50 mM sucrose). 100 µl of the Δcond extract were incubated twice with a half volume of the anti–topo IIα beads at 4°C for 30 min, and the supernatant was used as a condensin/topo II–depleted extract (Δcond Δtopo II extract).

Add-back assays and immunofluorescence analyses
Chromosome assembly assays using *Xenopus* egg extracts were performed as described previously (Kinoshita et al., 2015) with minor modifications. For standard add-back assays, Δcond extracts were supplemented with purified recombinant complexes (35 nM) and preincubated at 22°C for 15 min. *Xenopus* sperm nuclei were then added at a final concentration of 0.8–2.0 × 10³ nuclei/µl and incubated at 22°C for another 120 min to assemble chromosomes. Alternatively, mouse sperm nuclei prepared as described previously (Shintomi et al., 2017) were added at a final concentration of 0.4–1.0 × 10³ nuclei/µl and incubated at 22°C for 150 min. After incubation, the reaction mixtures were fixed

and processed for immunofluorescence analyses. For topo II–depleted add-back assays, Δcond Δtopo II extracts were used instead of Δcond extracts. Immunofluorescence analyses were performed as described previously (Kinoshita et al., 2015), except that an Olympus BX63 microscope equipped with a UPlanSApo 100×/1.40 NA oil immersion lens and an ORCA-Flash 4.0 digital complementary metal oxide semiconductor camera C11440 (Hamamatsu Photonics) were used for observations. CellSens Dimension software (Olympus) was used for image acquisition. Primary antibodies used for immunofluorescence in this study were as follows: anti-mSMC4, anti-histone H3, and anti–topo II.

Image analysis and statistics
Images acquired by immunofluorescence microscopy were subjected to quantitative analyses by using the ImageJ software (https://imagej.nih.gov/ij). For measurement of line profiles of chromosome axes, DAPI and SMC4 immunofluorescence signals on the scanned line were quantified by using the plot profile function. For quantification of the size of beans and cores, DAPI and SMC4 immunofluorescence signals were segmented by using the threshold function, and the signal-positive areas were measured using the function of analyzed particles. In the titration experiments of holo(H-III6Q) of ΔG(WT) concentrations, histone H3 immunofluorescence signals were used for the quantification of the bean size because the corresponding DAPI signals were too strong at high concentrations of the complexes to set a proper threshold for binarization. For measurement of the DNA intensity per DNA-positive area, DAPI signals were segmented by using the threshold function and the signal-positive areas, and the integrated densities were measured by using the function of analyzed particles. The integrated density was then divided by the area. The total number of images of a cluster of chromatids counted for each experiment for statistical analysis is described in the appropriate figure legends. All datasets were handled with Excel software (Microsoft), and the subsequent statistical analyses, curve fitting, and graph drawing were conducted using GraphPad Prism software (GraphPad Software). The data in Fig. 2, B and D, and Fig. 6, D–F and H–J, were analyzed using a two-tailed Mann-Whitney *U* test. The data in Fig. 5, E and G, are combined data from three independent experiments and are represented as SuperPlots to allow visualization of the data distribution in individual experiments (Lord et al., 2020). The aggregate data were then analyzed using a paired, two-tailed *t* test. Data distribution was assumed to be normal, but this was not formally tested.

Purification and labeling of Halo-tagged recombinant complexes
Halo-tagged versions of holo- and subcomplexes were purified by two-step column chromatography as described above. Peak fractions from HiTrap Q HP were concentrated, mixed with HaloTag Alexa Fluor 488 Ligand (Promega), and incubated at RT for 30 min. The labeled mixture was then loaded onto a PD-10 desalting column (Cytiva) to separate Alexa Fluor 488–labeled complexes from unbound ligands. The labeled complexes were

Kinoshita et al.
Chromosome shaping by condensin I

Journal of Cell Biology 15 of 17
https://doi.org/10.1083/jcb.202109016

concentrated with Amicon Ultra-15 (Merck Millipore), aliquoted, and stored at –80°C.

Mixing and pull-down experiments

To rule out the possibility that the partial rescue observed in the mixing experiment (Fig. 5) was caused by subunit exchange between the two different input complexes, the following pull-down experiment was set up. Two different complexes were prepared (Fig. S4 B): (1) HaloTag-holo(WT) including a HaloTag-conjugated version of CAP-H at its N terminus and the full-length version of CAP-D2 and (2) holo(D2-Δprb453-611) including an untagged version of CAP-H and a truncated version of CAP-D2. The use of the truncated version of CAP-D2 in complex 2 allowed us to distinguish it from the full-length version of CAP-D2. Both complexes 1 and 2 were confirmed to be functional in our add-back assay. For the pull-down experiment, a mixture of the two complexes was incubated with egg extracts (Δcond HSS) under the same condition as our standard add-back assay. After 90-min incubation at 22°C, the Magne HaloTag Beads (G7282; Promega), which covalently and specifically bind to HaloTag fusion proteins, were added and incubated for another 30 min at RT. The HaloTag beads were then collected and washed three times with XBE2. Finally, the bead-bound proteins were subjected to SDS-PAGE and analyzed by immunoblotting (Fig. S4 C).

Loop extrusion assay

A loop extrusion assay was performed by total internal reflection fluorescence microscopy as described previously (Sakata et al., 2021). Microfluidic flow cells that can switch the flow direction were used, and coverslips were coated with 1 mg/ml streptavidin in ELB++ (10 mM Hepes-KOH [pH 7.7], 50 mM KCl, 2.5 mM $MgCl_2$, 1 mg/ml BSA) for 30 min. After the flow cells were assembled, they were incubated with ELB++ for 30 min and then washed with 30 μl of T20 buffer (40 mM Tris-HCl [pH 7.5], 20 mM NaCl, 0.2 mM EDTA). Biotin-labeled λ-DNA in T20 buffer was attached to the coverslips for 5 min, and then unbound DNA was washed off with imaging buffer (50 mM Tris-HCl [pH 7.5], 50 mM NaCl, 5 mM $MgCl_2$, 3 mM ATP, 1 mM DTT) at the flow speed of 10 μl/min for 2 min. Then, the flow direction was switched, and the flow cells were washed with imaging buffer at 20 μl/min for 10 min. 1 nM condensin in imaging buffer was incubated at 30°C, introduced into the flow cells at 20 μl/min for 1.5 min, and washed off with imaging buffer at 20 μl/min. For visualization of Sytox Orange (22 nM)-stained DNA and Alexa Fluor 488–labeled condensin, 488-nm and 561-nm lasers were used, respectively. Images were taken every 5 s for 20 min after introducing condensin. The images were analyzed using ImageJ software. For the bleaching assay, flow cells were blocked with ELB++, then condensin was incubated for 5 min to allow binding nonspecifically to coverslips. Then, condensin was bleached by exposure to a 488-nm laser for 30 s, and images were taken every 0.5 s. Only one-step bleaching events were chosen and analyzed.

Animal use

Frogs were used in compliance with the institutional regulations of the RIKEN Wako Campus. Mice were used in compliance with

protocols approved by the animal care and use committee of the University of Tokyo (for M. Ohsugi).

Online supplemental material

Fig. S1 shows that holo(H-III4D) and holo(H-BC1/2D) produce structures similar to those produced by holo(H-III6Q) in the presence or absence of topo IIα. Fig. S2 illustrates the SMC ATPase cycle mutations and the method of subsequent addition of topo IIα to topo II–depleted extracts. Fig. S3 shows additional characterization of ΔG(WT)-mediated bean formation. Fig. S4 illustrates the D2-SMC4 contact mutations and provides evidence for the lack of subunit–subunit exchange in the mixing experiment. Fig. S5 provides additional information on the loop extrusion assay.

References

Alipour, E., and J.F. Marko. 2012. Self-organization of domain structures by DNA-loop-extruding enzymes. *Nucleic Acids Res.* 40:11202–11212. https://doi.org/10.1093/nar/gks925

Bayliss, R., T. Littlewood, and M. Stewart. 2000. Structural basis for the interaction between FxFG nucleoporin repeats and importin-β in nuclear trafficking. *Cell.* 102:99–108. https://doi.org/10.1016/S0092-8674(00)00014-3

Bayliss, R., T. Littlewood, L.A. Strawn, S.R. Wente, and M. Stewart. 2002. GLFG and FxFG nucleoporins bind to overlapping sites on

importin-β. *J. Biol. Chem.* 277:50597–50606. https://doi.org/10.1074/jbc.M209037200

Cheng, T.M., S. Heeger, R.A. Chaleil, N. Matthews, A. Stewart, J. Wright, C. Lim, P.A. Bates, and F. Uhlmann. 2015. A simple biophysical model emulates budding yeast chromosome condensation. *eLife.* 4:e05565. https://doi.org/10.7554/eLife.05565

Davidson, I.F., B. Bauer, D. Goetz, W. Tang, G. Wutz, and J.M. Peters. 2019. DNA loop extrusion by human cohesin. *Science.* 366:1338–1345. https://doi.org/10.1126/science.aaz3418

Eng, T., V. Guacci, and D. Koshland. 2015. Interallelic complementation provides functional evidence for cohesin-cohesin interactions on DNA. *Mol. Biol. Cell.* 26:4224–4235. https://doi.org/10.1091/mbc.e15-06-0331

Ganji, M., I.A. Shaltiel, S. Bisht, E. Kim, A. Kalichava, C.H. Haering, and C. Dekker. 2018. Real-time imaging of DNA loop extrusion by condensin. *Science.* 360:102–105. https://doi.org/10.1126/science.aar7831

Gerguri, T., X. Fu, Y. Kakui, B.S. Khatri, C. Barrington, P.A. Bates, and F. Uhlmann. 2021. Comparison of loop extrusion and diffusion capture as mitotic chromosome formation pathways in fission yeast. *Nucleic Acids Res.* 49:1294–1312. https://doi.org/10.1093/nar/gkaa1270

Gibcus, J.H., K. Samejima, A. Goloborodko, I. Samejima, N. Naumova, J. Nuebler, M.T. Kanemaki, L. Xie, J.R. Paulson, W.C. Earnshaw, et al. 2018. A pathway for mitotic chromosome formation. *Science.* 359: eaao6135. https://doi.org/10.1126/science.aao6135

Goloborodko, A., M.V. Imakaev, J.F. Marko, and L. Mirny. 2016a. Compaction and segregation of sister chromatids via active loop extrusion. *eLife.* 5: e14864. https://doi.org/10.7554/eLife.14864

Goloborodko, A., J.F. Marko, and L.A. Mirny. 2016b. Chromosome compaction by active loop extrusion. *Biophys. J.* 110:2162–2168. https://doi.org/10.1016/j.bpj.2016.02.041

Hara, K., K. Kinoshita, T. Migita, K. Murakami, K. Shimizu, K. Takeuchi, T. Hirano, and H. Hashimoto. 2019. Structural basis of HEAT-kleisin interactions in the human condensin I subcomplex. *EMBO Rep.* 20:e47183. https://doi.org/10.15252/embr.201847183

Hassler, M., I.A. Shaltiel, M. Kschonsak, B. Simon, F. Merkel, L. Thärichen, H.J. Bailey, J. Macošek, S. Bravo, J. Metz, et al. 2019. Structural basis of an asymmetric condensin ATPase cycle. *Mol. Cell.* 74:1175–1188.e9. https://doi.org/10.1016/j.molcel.2019.03.037

Hirano, T. 2014. Condensins and the evolution of torsion-mediated genome organization. *Trends Cell Biol.* 24:727–733. https://doi.org/10.1016/j.tcb.2014.06.007

Hirano, T. 2016. Condensin-based chromosome organization from bacteria to vertebrates. *Cell.* 164:847–857. https://doi.org/10.1016/j.cell.2016.01.033

Hirano, T., and T.J. Mitchison. 1993. Topoisomerase II does not play a scaffolding role in the organization of mitotic chromosomes assembled in *Xenopus* egg extracts. *J. Cell Biol.* 120:601–612. https://doi.org/10.1083/jcb.120.3.601

Hirano, T., and T.J. Mitchison. 1994. A heterodimeric coiled-coil protein required for mitotic chromosome condensation in vitro. *Cell.* 79:449–458. https://doi.org/10.1016/0092-8674(94)90254-2

Hirano, T., R. Kobayashi, and M. Hirano. 1997. Condensins, chromosome condensation protein complexes containing XCAP-C, XCAP-E and a *Xenopus* homolog of the *Drosophila* Barren protein. *Cell.* 89:511–521. https://doi.org/10.1016/S0092-8674(00)80233-0

Keenholtz, R.A., T. Dhanaraman, R. Palou, J. Yu, D. D'Amours, and J.F. Marko. 2017. Oligomerization and ATP stimulate condensin-mediated DNA compaction. *Sci. Rep.* 7:14279. https://doi.org/10.1038/s41598-017-14701-5

Kim, Y., Z. Shi, H. Zhang, I.J. Finkelstein, and H. Yu. 2019. Human cohesin compacts DNA by loop extrusion. *Science.* 366:1345–1349. https://doi.org/10.1126/science.aaz4475

Kinoshita, K., T.J. Kobayashi, and T. Hirano. 2015. Balancing acts of two HEAT subunits of condensin I support dynamic assembly of chromosome axes. *Dev. Cell.* 33:94–106. https://doi.org/10.1016/j.devcel.2015.01.034

Kong, M., E.E. Cutts, D. Pan, F. Beuron, T. Kaliyappan, C. Xue, E.P. Morris, A. Musacchio, A. Vannini, and E.C. Greene. 2020. Human condensin I and II drive extensive ATP-dependent compaction of nucleosome-bound DNA. *Mol. Cell.* 79:99–114.e9. https://doi.org/10.1016/j.molcel.2020.04.026

Kschonsak, M., F. Merkel, S. Bisht, J. Metz, V. Rybin, M. Hassler, and C.H. Haering. 2017. Structural basis for a safety-belt mechanism that anchors condensin to chromosomes. *Cell.* 171:588–600.e24. https://doi.org/10.1016/j.cell.2017.09.008

Lee, J., S. Ogushi, M. Saitou, and T. Hirano. 2011. Condensins I and II are essential for construction of bivalent chromosomes in mouse oocytes. *Mol. Biol. Cell.* 22:3465–3477. https://doi.org/10.1091/mbc.e11-05-0423

Lee, B.G., F. Merkel, M. Allegretti, M. Hassler, C. Cawood, L. Lecomte, F.J. O'Reilly, L.R. Sinn, P. Gutierrez-Escribano, M. Kschonsak, et al. 2020. Cryo-EM structures of holo condensin reveal a subunit flip-flop mechanism. *Nat. Struct. Mol. Biol.* 27:743–751. https://doi.org/10.1038/s41594-020-0457-x

Liu, S.M., and M. Stewart. 2005. Structural basis for the high-affinity binding of nucleoporin Nup1p to the *Saccharomyces cerevisiae* importin-β homologue, Kap95p. *J. Mol. Biol.* 349:515–525. https://doi.org/10.1016/j.jmb.2005.04.003

Lord, S.J., K.B. Velle, R.D. Mullins, and L.K. Fritz-Laylin. 2020. SuperPlots: communicating reproducibility and variability in cell biology. *J. Cell Biol.* 219:e202001064. https://doi.org/10.1083/jcb.202001064

Losada, A., M. Hirano, and T. Hirano. 1998. Identification of *Xenopus* SMC protein complexes required for sister chromatid cohesion. *Genes Dev.* 12: 1986–1997. https://doi.org/10.1101/gad.12.13.1986

Nasmyth, K. 2001. Disseminating the genome: joining, resolving, and separating sister chromatids during mitosis and meiosis. *Annu. Rev. Genet.* 35:673–745. https://doi.org/10.1146/annurev.genet.35.102401.091334

Ono, T., A. Losada, M. Hirano, M.P. Myers, A.F. Neuwald, and T. Hirano. 2003. Differential contributions of condensin I and condensin II to mitotic chromosome architecture in vertebrate cells. *Cell.* 115:109–121. https://doi.org/10.1016/S0092-8674(03)00724-4

Paulson, J.R., D.F. Hudson, F. Cisneros-Soberanis, and W.C. Earnshaw. 2021. Mitotic chromosomes. *Semin. Cell Dev. Biol.* 117:7–29. https://doi.org/10.1016/j.semcdb.2021.03.014

Piazza, I., A. Rutkowska, A. Ori, M. Walczak, J. Metz, V. Pelechano, M. Beck, and C.H. Haering. 2014. Association of condensin with chromosomes depends on DNA binding by its HEAT-repeat subunits. *Nat. Struct. Mol. Biol.* 21:560–568. https://doi.org/10.1038/nsmb.2831

Ryu, J.K., A.J. Katan, E.O. van der Sluis, T. Wisse, R. de Groot, C.H. Haering, and C. Dekker. 2020. The condensin holocomplex cycles dynamically between open and collapsed states. *Nat. Struct. Mol. Biol.* 27:1134–1141. https://doi.org/10.1038/s41594-020-0508-3

Ryu, J.K., C. Bouchoux, H.W. Liu, E. Kim, M. Minamino, R. de Groot, A.J. Katan, A. Bonato, D. Marenduzzo, D. Michieletto, et al. 2021. Bridging-induced phase separation induced by cohesin SMC protein complexes. *Sci. Adv.* 7:eabe5905. https://doi.org/10.1126/sciadv.abe5905

Sakai, Y., A. Mochizuki, K. Kinoshita, T. Hirano, and M. Tachikawa. 2018. Modeling the functions of condensin in chromosome shaping and segregation. *PLOS Comput. Biol.* 14:e1006152. https://doi.org/10.1371/journal.pcbi.1006152

Sakata, R., K. Niwa, D. Ugarte La Torre, C. Gu, E. Tahara, S. Takada, and T. Nishiyama. 2021. Opening of cohesin's SMC ring is essential for timely DNA replication and DNA loop formation. *Cell Rep.* 35:108999. https://doi.org/10.1016/j.celrep.2021.108999

Shintomi, K., and T. Hirano. 2021. Guiding functions of the C-terminal domain of topoisomerase IIα advance mitotic chromosome assembly. *Nat. Commun.* 12:2917. https://doi.org/10.1038/s41467-021-23205-w

Shintomi, K., T.S. Takahashi, and T. Hirano. 2015. Reconstitution of mitotic chromatids with a minimum set of purified factors. *Nat. Cell Biol.* 17: 1014–1023. https://doi.org/10.1038/ncb3187

Shintomi, K., F. Inoue, H. Watanabe, K. Ohsumi, M. Ohsugi, and T. Hirano. 2017. Mitotic chromosome assembly despite nucleosome depletion in *Xenopus* egg extracts. *Science.* 356:1284–1287. https://doi.org/10.1126/science.aam9702

Tedeschi, A., G. Wutz, S. Huet, M. Jaritz, A. Wuensche, E. Schirghuber, I.F. Davidson, W. Tang, D.A. Cisneros, V. Bhaskara, et al. 2013. Wapl is an essential regulator of chromatin structure and chromosome segregation. *Nature.* 501:564–568. https://doi.org/10.1038/nature12471

Terakawa, T., S. Bisht, J.M. Eeftens, C. Dekker, C.H. Haering, and E.C. Greene. 2017. The condensin complex is a mechanochemical motor that translocates along DNA. *Science.* 358:672–676. https://doi.org/10.1126/science.aan6516

Uhlmann, F. 2016. SMC complexes: from DNA to chromosomes. *Nat. Rev. Mol. Cell Biol.* 17:399–412. https://doi.org/10.1038/nrm.2016.30

Xiang, S., and D. Koshland. 2021. Cohesin architecture and clustering in vivo. *eLife.* 10:e62243. https://doi.org/10.7554/eLife.62243

Yoshimura, S.H., and T. Hirano. 2016. HEAT repeats – versatile arrays of amphiphilic helices working in crowded environments? *J. Cell Sci.* 129: 3963–3970. https://doi.org/10.1242/jcs.185710

Yoshimura, S.H., M. Kumeta, and K. Takeyasu. 2014. Structural mechanism of nuclear transport mediated by importin β and flexible amphiphilic proteins. *Structure.* 22:1699–1710. https://doi.org/10.1016/j.str.2014.10.009
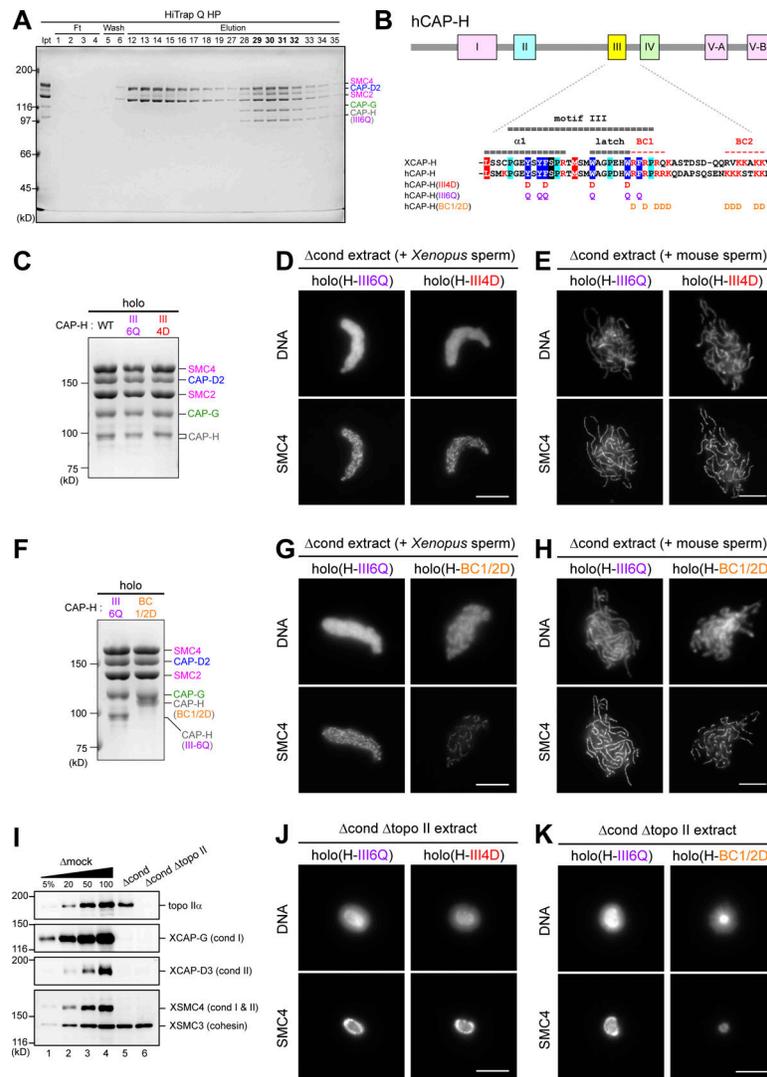
Supplemental material

Figure S1.   **Holo(H-III4D) and holo(H-BC1/2D) produce structures similar to those produced by holo(H-III6Q) in the presence or absence of topo IIα.** **(A)** Purification of the condensin I holocomplex harboring the H-III6Q mutations by HiTrap Q HP. Fractions released from a glutathione affinity column were pooled and subjected to a HiTrap Q HP column. Protein samples at each step were subjected to SDS-PAGE, and the gel was stained with Coomassie brilliant blue (CBB; input [ipt]; flowthrough [Ft]; wash fractions [Wash]; elution fractions [Elution]). Peak fractions (elution fractions 29–32) were pooled, concentrated, aliquoted, and stored at −80°C. **(B)** The III4D and BC1/2D mutations of CAP-H. The III4D mutations of CAP-H were an equivalent to the ϕD mutations of budding yeast Brn1 that were designed by Kschonsak et al. (2017). BC1 and BC2, positively charged patches present in motif III, were identified as subregions that are required for DNA binding by the CAP-H/Brn1 subunit (Kschonsak et al., 2017). The BC1/2D mutations were created by substituting all basic residues (K/R) conserved in BC1 and BC2 with aspartic acid residues (D). **(C)** The WT and two motif III mutant complexes (H-III6Q and H-III4D) were purified and subjected to SDS-PAGE. The gel was stained with CBB. **(D)** Add-back assay using *Xenopus* sperm nuclei as a substrate. *Xenopus* sperm nuclei were incubated with condensin-depleted (Δcond) extracts that had been supplemented with holo(H-III6Q) or holo(H-III4D). After 120 min, the reaction mixtures were fixed and labeled with an antibody against SMC4. DNA was counterstained with DAPI. Scale bar, 10 µm. **(E)** Add-back assay using mouse sperm nuclei as a substrate. Mouse sperm nuclei were incubated with the same set of extracts as described in D for 150 min and analyzed as above. Scale bar, 10 µm. **(F)** Holo(H-III6Q) and holo(H-BC1/2D) were purified and subjected to SDS-PAGE. The gel was stained with CBB. **(G)** Add-back assay using *Xenopus* sperm nuclei as a substrate. *Xenopus* sperm nuclei were incubated with condensin-depleted (Δcond) extracts that had been supplemented with holo(H-III6Q) or holo(H-BC1/2D). After 120 min, the reaction mixtures were fixed and labeled with an antibody against SMC4. DNA was counterstained with DAPI. We noticed that the banana-shaped structures produced by holo(H-BC1/2D) were slightly thicker than those produced by holo(H-III6Q). Scale bar, 10 µm. **(H)** Add-back assay using mouse sperm nuclei as a substrate. Mouse sperm nuclei were incubated with the same set of extracts as described in G for 150 min and analyzed as above. We noticed that the axis structures produced by holo(H-BC1/2D) were less continuous than those produced by holo(H-III6Q). Scale bar, 10 µm. **(I)** Immunodepletion. *Xenopus* egg extracts were immunodepleted with control IgG (Δmock), antibodies against condensin subunits (Δcond), or a mixture of antibodies against condensin subunits and topo IIα (Δcond Δtopo II; see Materials and methods for details). To estimate the efficiency of immunodepletion, an aliquot of each extract along with decreasing amounts of the Δmock extract (100, 50, 20, and 5%) were analyzed with the antibodies indicated. *Xenopus* SMC3 (XSMC3), a subunit of the cohesin complex, was used as a loading control. **(J)** Topo II–depleted add-back assay using mouse sperm nuclei as a substrate. Mouse sperm nuclei were incubated with Δcond Δtopo II extracts that had been supplemented with holo(H-III6Q) or holo(H-III4D). After 150 min, the reaction mixtures were fixed and labeled with an antibody against SMC4. DNA was counterstained with DAPI. Scale bar, 10 µm. **(K)** Topo II–depleted add-back assay using mouse sperm nuclei as a substrate. Mouse sperm nuclei were incubated with Δcond Δtopo II extracts that had been supplemented with holo(H-III6Q) or holo(H-BC1/2D) for 150 min and analyzed as above. Scale bar, 10 µm.
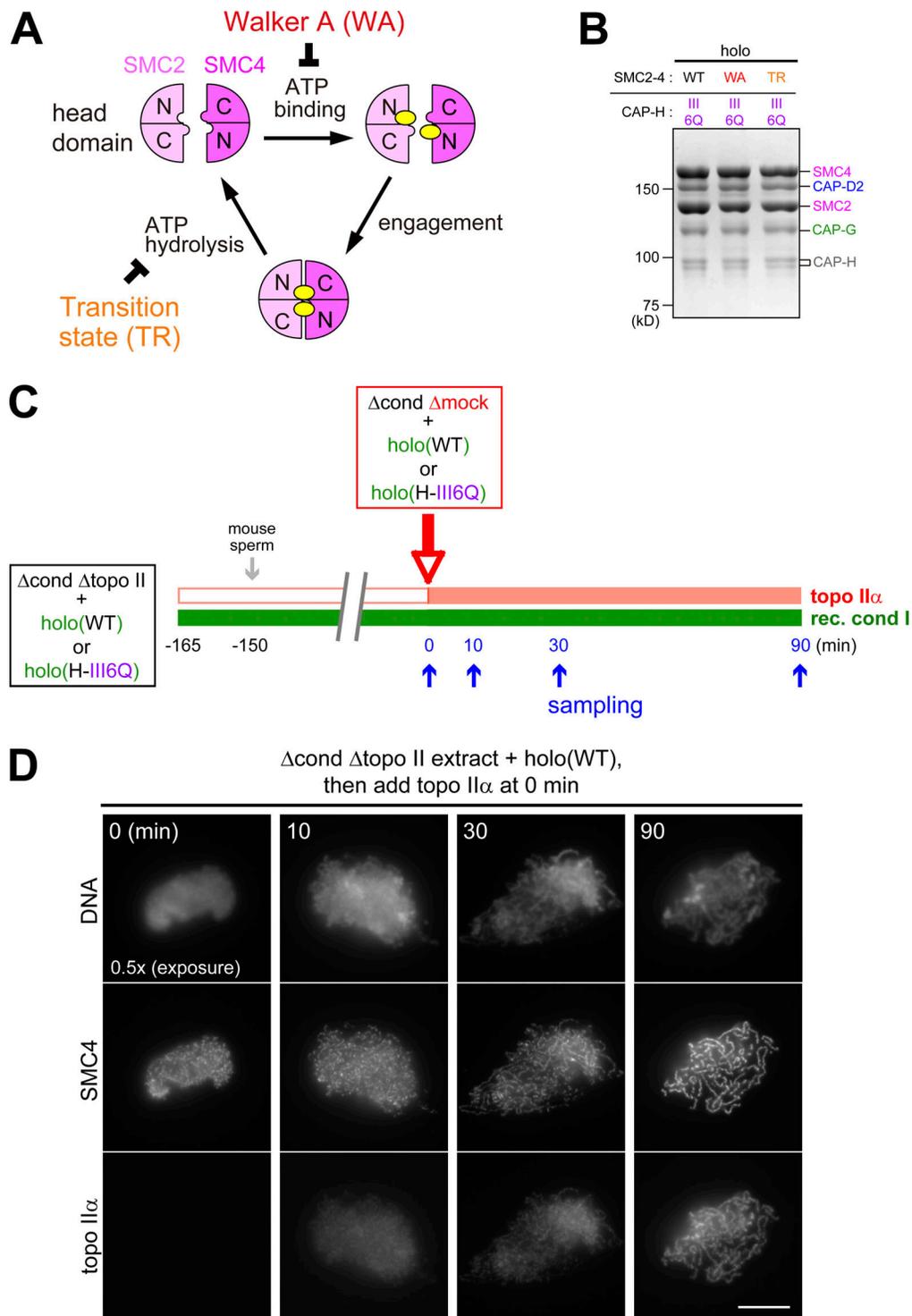
Figure S2.   **SMC ATPase cycle mutations and subsequent addition of topo IIα to topo II–depleted extracts. (A)** A schematic view of the SMC ATPase cycle. Two ATP molecules are sandwiched between the head domains of SMC2 and SMC4, and engagement of the ATP-bound head domains triggers ATP hydrolysis. The Walker A mutations (WA) block ATP binding, whereas the transition state mutations (TR) greatly slow the rate of ATP hydrolysis. **(B)** The H-III6Q mutant holocomplexes harboring WT or ATPase mutations (WA or TR) in the SMC2–4 subunits were purified and subjected to SDS-PAGE. The gel was stained with CBB. **(C)** Experimental procedure for subsequent add-back of topo II. Extracts depleted of both condensins and topo IIα (Δcond Δtopo II) were supplemented with holo(WT) or holo(H-III6Q) at −165 min. After 15-min preincubation, mouse sperm nuclei were incubated with the extracts for 150 min to form chromatin masses or beans, respectively. Then Δcond extracts that had been supplemented with holo(WT) or holo(H-III6Q) were added at 0 min. Aliquots were taken at the time intervals indicated, fixed, and processed for immunofluorescence. **(D)** Add-back of topo IIα after chromatin mass formation. A reaction with holo(WT) was set up as described in C. Aliquots were taken at the time intervals indicated, fixed, and processed for immunofluorescence with antibodies against SMC4 and topo IIα. DNA was counterstained with DAPI. The DAPI image of the structure produced at 0 min was taken with a shorter exposure time (0.5x) than the others. Scale bar, 10 μm.
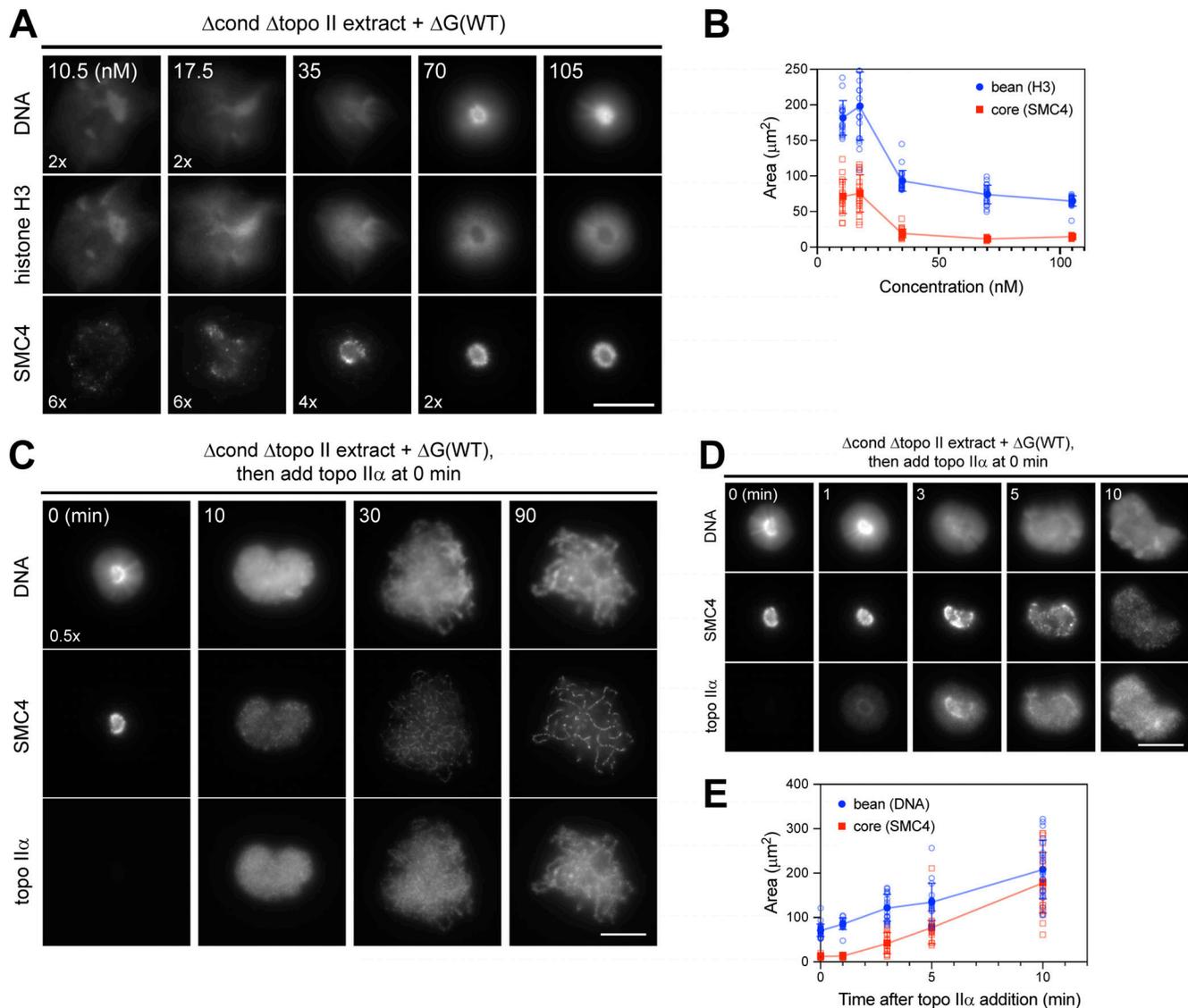
Figure S3. **Additional characterization of ΔG(WT)-mediated bean formation. (A)** Titration of ΔG(WT) in a topo II–depleted add-back assay. Mouse sperm nuclei were incubated with Δcond Δtopo II extracts that had been supplemented with the indicated concentrations of ΔG(WT). After 150 min, the reaction mixtures were fixed and labeled with antibodies against histone H3 and SMC4. DNA was counterstained with DAPI. Different relative exposure times were used wherever indicated (2x, 4x, or 6x). Scale bar, 10 μm. **(B)** Quantification of histone H3-positive (bean, shown in blue) and SMC4-positive (core, shown in red) areas in the structures shown in A. The mean and SD are shown (*n* = 17, 20, 24, 21, and 25 from 10.5 to 105 nM). **(C)** Add-back of topo IIα after bean formation by ΔG(WT). Mouse sperm nuclei were mixed with a Δcond Δtopo II extract had been supplemented with ΔG(WT) and incubated for 150 min to form beans. A Δcond extract that had been supplemented with ΔG(WT) was added at 0 min. Aliquots were taken at the time points indicated, fixed, and processed for immunofluorescence with antibodies against SMC4 and topo IIα. DNA was counterstained with DAPI. A different relative exposure time (0.5x) was used where indicated. Scale bar, 10 μm. **(D)** Add-back of topo IIα after bean formation by ΔG(WT). The same assembly mixture was set up as in C, but aliquots were taken at the earlier time points indicated and analyzed as above. Scale bar, 10 μm. **(E)** Quantification of DNA-positive (bean, shown in blue) and SMC4-positive (core, shown in red) areas in the structures shown in D. The mean and SD are shown (*n* = 28, 15, 17, 18, and 21 from 0 to 10 min).
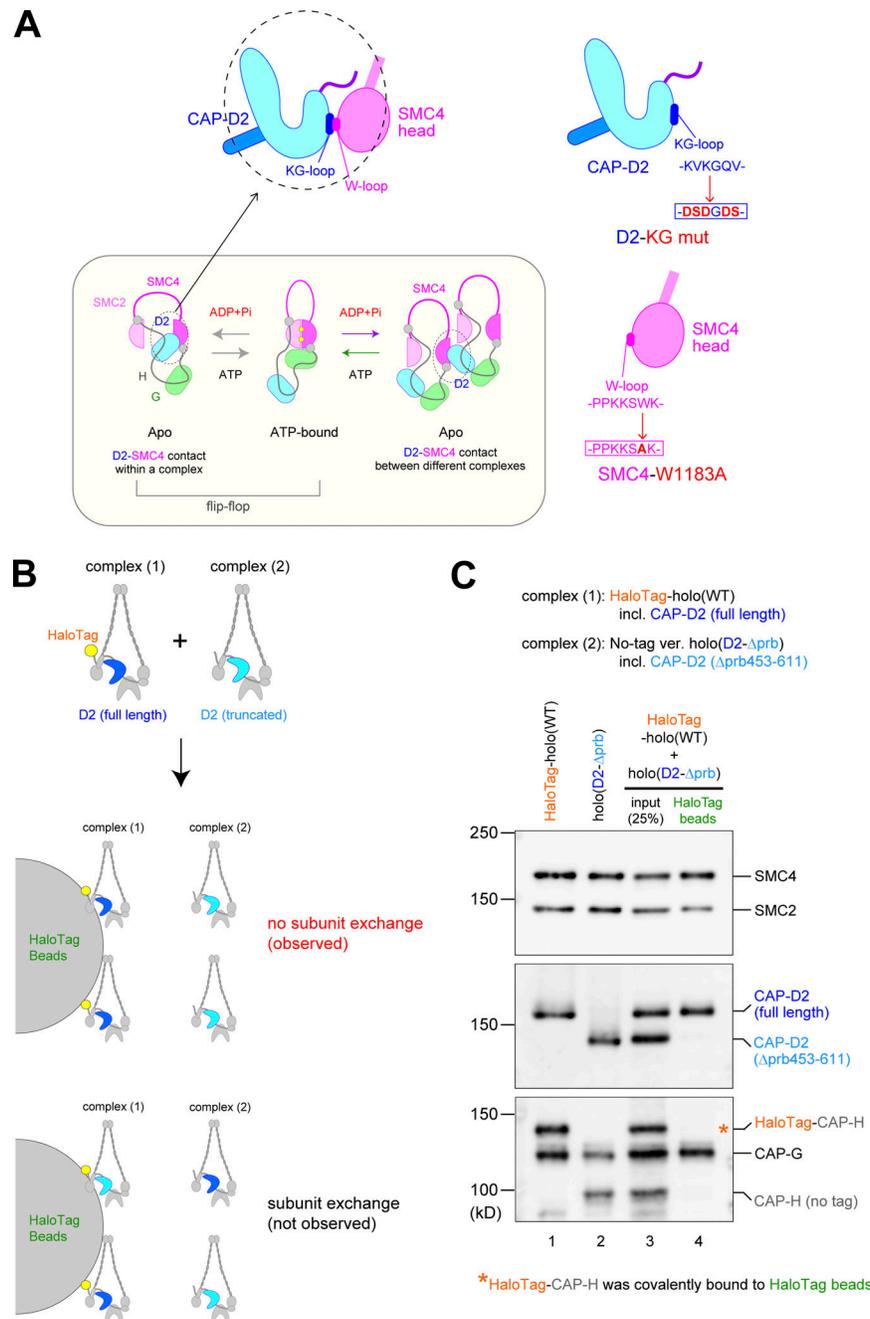
Figure S4. **The D2-SMC4 contact mutations and evidence for the lack of subunit–subunit exchange in the mixing experiment. (A)** A schematic view of the D2-SMC4 contact originally reported by Hassler et al. (2019), in which the KG-loop of CAP-D2/Ycs4 and the W-loop of SMC4/Smc4 make a contact in the absence of ATP (Hassler et al., 2019; left, top). Upon ATP binding, CAP-D2 is released from SMC4, allowing ATP-dependent engagement between the SMC2 and SMC4 head domains. Together with cryo-EM studies, a so-called flip-flop mechanism of the condensin reaction cycle has been proposed (Lee et al., 2020; left, bottom). In the present study, we hypothesize that, under crowded conditions, the D2-SMC4 contact could occur not only within individual complexes but also between different complexes. The KG-loop mutations (KG mut) of CAP-D2 and the W-loop mutation (W1183A) of SMC4 were designed (right) based on the corresponding yeast mutations reported by Hassler et al. (2019). **(B)** Experimental design to rule out the possibility that the partial rescue observed in the mixing experiment (Fig. 5) was caused by subunit exchange between the two different input complexes. A mixture of complexes 1 and 2 (see Materials and methods for details) was incubated with egg extracts (Δcond extract) under the same condition as the standard add-back assay, and the Halo-tagged CAP-H was recovered on the Magne HaloTag Beads. If no subunit exchange occurred in the egg extracts, the truncated version of CAP-D2 would not be recovered on the beads (no subunit exchange). If subunit exchange occurred in the egg extracts, the truncated version in addition to the full-length version of CAP-D2 would be recovered on the beads (subunit exchange). **(C)** Experimental result. Two purified complexes (lanes 1 and 2), a mixture of the two complexes in Δcond extract (lane 3) and a HaloTag bead-bound fraction recovered from the mixture (lane 4), were subjected to SDS-PAGE followed by immunoblotting with the antibodies indicated. We found that the full-length CAP-D2 present in the HaloTag-conjugated complex 1 was efficiently recovered, whereas the truncated version of CAP-D2 present in complex 2 was barely detectable in the bead-bound fraction. Likewise, the untagged version of CAP-H present in complex 2 was not recovered. (Note that the HaloTag-conjugated CAP-H in complex 1 was not detectable in lane 4, because it was covalently bound to the HaloTag beads.) This result demonstrated that subunit exchange between different condensin complexes barely occurs in egg extracts under our experimental condition.
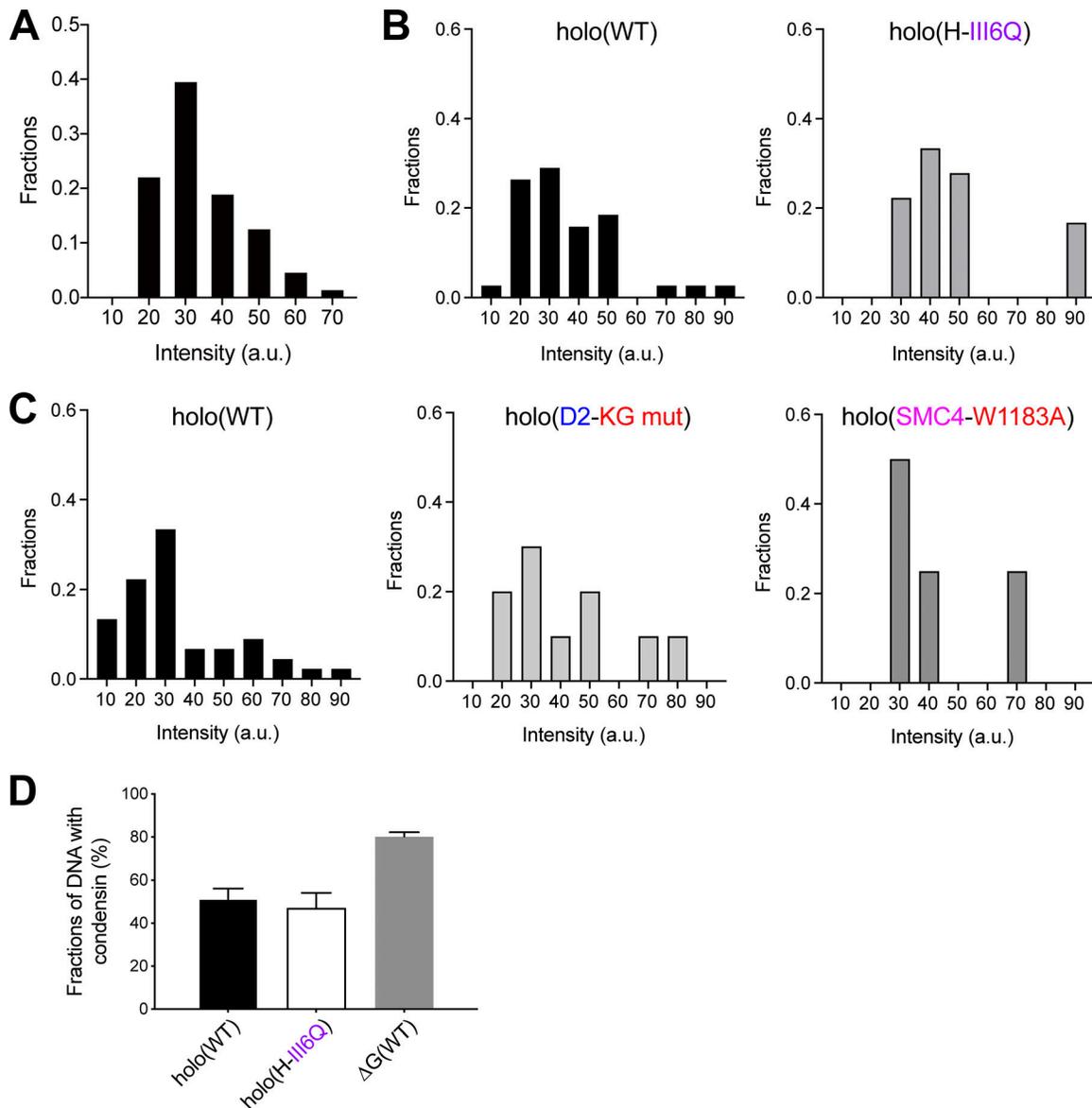
Figure S5. **Additional information on the loop extrusion assay. (A)** Fluorescence intensity distribution of labeled holo(WT). Time traces of the condensin intensity were taken from a bleaching experiment. Shown here is the distribution of the intensities that were bleached in one step. 61 particles were analyzed in total. **(B)** Fluorescence intensity distribution of holo(WT) or holo(H-III6Q) signals localized at the base of loops (from five independent experiments, n = 40 [holo[WT]] and 22 [holo[H-III6Q]]). **(C)** Fluorescence intensity distribution of holo(WT), holo(D2-KG mut), or holo(SMC4-W1183A) signals localized at the base of loops (from three independent experiments, n = 52 [holo[WT]], 14 [holo[D2-KG mut]], and 8 [holo[SMC4-W1183A]]). **(D)** Fractions of DNA with condensin bound in the first set of experiments shown in Fig. 6 C (from five independent experiments, n = 427 [holo[WT]], 423 [holo[H-III6Q]], and 543 [ΔG[WT]]; mean ± SEM).